https://doi.org/10.5194/egusphere-2025-2515
Preprint. Discussion started: 10 July 2025

Last Glacial Maximum extent and subsequent retreat of the East Antarctic Ice Sheet from the Mac. Robertson Shelf

Janina Güntzel[1,2], Juliane Müller[1,3], Ralf Tiedemann[1,2], Gesine Mollenhauer[1,2,3], Lester Lembke-Jene[1], Estella Weigelt[1], Lasse Schopen[2], Niklas Wesch[2], Laura Kattein[1], Andrew Mackintosh[4] and Johann P. Klages[1,3]

[1]Department of Geosciences, Alfred Wegener Institute Helmholtz Centre for Polar and Marine Research, Bremerhaven, Germany
[2]Department of Geosciences, University of Bremen, Bremen, Germany
[3]Cluster of Excellence "The Ocean Floor – Earth's Uncharted Interface", University of Bremen, Germany
[4]Securing Antarctica's Environmental Future, School of Earth, Atmosphere and Environment, Monash University, Victoria, Australia.

Correspondence to: Janina Güntzel (janina.guentzel@awi.de)

Abstract. The future behavior of the Antarctic Ice Sheet is considered to be one of the largest unknowns in global climate projections, with dramatically accelerating ice loss being observed over the past few decades in multiple drainage basins. However, those records only reflect a short moment of limited informative value when considering the length of a full cycle of ice sheet expansion and retreat. East Antarctica's deglaciation history remains largely understudied compared to the West Antarctic margin. This emphasizes the urgent need for reliable long-term spatiotemporal data on ice sheet change, particularly for sectors that play key roles in supplying the world's oceans with dense bottom water. In this study, we performed a multi-proxy analysis on a set of sediment cores recovered from two prominent glacial cross-shelf troughs on the Mac. Robertson Shelf. We classified submarine glacial landforms on the shelf along both troughs from combined multibeam swath bathymetry and sub-bottom profiler data to infer ice sheet retreat dynamics. Additionally, combined sedimentological, sediment-physical, and geochemical analyses, including radiocarbon ages of foraminifera, reveal the onset of deglaciation on the Mac. Robertson Shelf and the subsequent retreat of the grounding line (GL). Glacial bedforms indicate an episodic retreat of the ice sheet's GL, which started with a slow retreat on the outer shelf and accelerated towards the retrograde mid-shelf part. Across the mid-shelf, the GL repeatedly halted, leading to the formation of several small grounding-zone wedges. A mid-shelf bedrock sill likely acted as a pinning point, indicating an additional grounding line stabilization period. Our study reveals that the grounding line advanced to the continental shelf break prior to ~12.5 cal. ka BP, which prevented the formation of dense shelf water on the Mac. Robertson Shelf in its current form and, therefore, suggests either an absent or a different formation mechanism of Antarctic Bottom Water under full glacial conditions. Further, we conclude a retreat at or shortly after the Antarctic Cold Reversal ~12,5 calibrated kiloyears before the present (i.e., 1950 CE, cal. ka BP) from the outer shelf.

https://doi.org/10.5194/egusphere-2025-2515
Preprint. Discussion started: 10 July 2025

1 Introduction

Antarctica's grounded ice sheets are characterized by ice streams and outlet glaciers, which drain ice from the interior toward the ocean (e.g. Rignot et al., 2011). The East Antarctic Ice Sheet (EAIS) is the largest ice sheet on Earth, situated mostly above sea level. In contrast, major parts of the West Antarctic Ice Sheet (WAIS) are grounded below sea level (Fretwell et al., 2013, Pritchard et al., 2025), making it inherently unstable and prone to melting at its base, potentially inducing a retreat of the grounding line (Schoof et al., 2007). Ice mass loss has accelerated significantly over the last decades, with dominant losses from West Antarctica (e.g. Rignot et al., 2019). However, the cumulative contribution to sea level rise from the East Antarctic Ice Sheet (EAIS) is assumed to have recently caught up with that from the WAIS (e.g., Rignot et al., 2019; The IMBIE Team 2018). Especially, regions located on retrograde slopes in submarine basins, such as the Wilkes Land in East Antarctica with major basins below sea level, are at higher risk for so-called marine ice sheet instabilities (MISI) (Schoof et al., 2007; Pritchard et al., 2025).

The grounding zone of an ice sheet, where the ice meets the ocean at the grounding line (GL), is a critical region in terms of ice sheet instability. Hence, information on the processes and dynamics of GL retreat patterns is crucial for a better understanding of the effects of sea level rise on ice retreat and to improve future predictions (e.g. Bradley and Hewitt, 2024). The AIS likely extended towards outer continental shelf regions during the Last Glacial Maximum (LGM) and retreated to or near modern positions by 5 cal. ka BP (RAISED Consortium, 2014). However, they concluded that positions and timing of the subsequent grounding line (GL) retreat towards innermost shelf regions remain poorly constrained for most areas, particularly along the East Antarctic margin (Mackintosh et al., 2014).

In our study, we investigated the spatiotemporal extent and retreat of the GL across the Mac. Robertson Shelf, where dense shelf water (DSW) currently forms due to brine rejection from sea ice formation in coastal polynyas. From here, it eventually flows down the continental slope, mixing with CDW and contributing to Antarctic Bottom Water (AABW) formation (e.g., Wong and Riser, 2013; Schmidt et al., 2023). AABW is the world's ocean densest water mass and a major component of the ocean's overturning circulation (e.g., Ohshima et al., 2013). Only recently, parts of the continental shelf offshore the Mac. Robertson Land have been recognized as an important additional source region for AABW with approximately 20 – 25% modified Shelf Water production (Wong and Riser, 2013; Mizuta et al., 2024). This makes it highly relevant to reliably assess whether or not the shelf was covered by grounded ice during the LGM, i.e., if AABW formed there via the modern formation mechanism, with direct implications for better understanding circum-Antarctic Ocean circulation during past glacial maxima. We present a multi-proxy approach on several sediment cores recovered from two major cross-shelf glacial troughs – Nielsen Basin and Iceberg Alley, Mac. Robertson Shelf (Fig. 1, 2) to identify the maximum ice sheet extent and the initial GL retreat and pattern of the subsequent retreat by combining our geophysical and geological data of these cores retrieved from the Mac. Robertson Shelf during the RV *Polarstern* Expedition 2022. We present a framework for the timing of initial deglaciation since the Last Glacial Maximum, here ~ 19,000 to 25,000 years ago, which provides essential information to complete the deglacial history of the Mac. Robertson Shelf. The timing of deglaciation for the Mac. Robertson Shelf since the LGM was set

https://doi.org/10.5194/egusphere-2025-2515
Preprint. Discussion started: 10 July 2025

between 14.0 and 12.0 cal. ka BP by previously measured AMS ^{14}C and cosmogenic ^{10}Be and ^{26}Al dates (Mackintosh et al., 2007; Leventer et al., 2006) as well as the integration of onshore and offshore evidence with ice sheet modelling (Mackintosh et al., 2011). Our combined facies analysis with radiocarbon dates of calcareous microfossils revealed the onset of deglaciation on the Mac. Robertson Shelf and the maximum GL position with its retreat patterns since the LGM. Our data, therefore, provide new evidence on the initial grounding-line retreat since the last glacial maximum and the nature of the ice retreat and we propose that a shut-off of DSW production on the Mac. Robertson Shelf suggests either an absent or a different DSW formation mechanism under full glacial conditions, with implications for AABW formation.

2 Study area

The geomorphology of the East Antarctic Shelf is typical for glaciated continental margins with outer shelf banks, cross-cutting deeper troughs and inner-shelf deeps, which are mostly overdeepened. This shelf geomorphology affects the dynamics of the ice sheet. The Framnes Mountains, located in the hinterland of the Mac. Robertson Shelf, consists of a series of ice-free nunataks and ranges, characterised by ice-free bedrock and glacial sediments (Mackintosh et al., 2007). As part of the East Antarctic craton, the prominent found on the Mac. Robertson Land are magmatic protoliths and tonalitic orthogneisses ~3,100-2,800 Ma ago. It is bordered by the Amery ice shelf towards the East and the Kemp Land and Enderby Land to the West (Fig.1). The shelf area is bounded by the Indian Ocean to the East and by the Cooperation Sea to the West. It is relatively narrow, < 90 km wide, and comprises shallow banks cut by deeper troughs (Leventer et al., 2006). The prevailing currents in that area are the Antarctic Coastal Current (ACoC), which rotates counter-clockwise around the coasts of the Antarctic continent and the Antarctic Circumpolar Current (ACC), which circulates the continent in a clockwise direction. (Fig.1).
The most prominent macroscale geomorphic features on the Mac. Robertson Shelf are two glacial troughs, the Nielsen Basin and Iceberg Alley. Those basins were suggested to be major pathways of fast-flowing ice during the last glacial (Leventer et al., 2006; Mackintosh et al., 2011). Nielsen Basin is more sinuous in shape and with a maximum depth of around 1300 mbsl, deeper than Iceberg Alley. However, both troughs show a similar relief commonly found in Antarctic shelf basins. (Leventer et al., 2006; Fig.2). The outer shelf areas of both troughs are characterized by shallow water depths around ~300-500 m (Harris and O'Brien, 1998; Sedwick et al., 2001). Mackintosh et al. (2011) identified two grounding zone wedges (GZW) on the outer shelf of Nielsen Basin and Iceberg Alley by geophysical investigations, which are thought to mark the most recent expansion of the ice sheet onto the continental shelf at equal water depths (388 mbsl) in both troughs (Fig.2).

The newly described Cape Darnley Bottom Water (CDBW) is produced in the Cape Darnley polynya, which is located on the seaward side of a grounded iceberg tongue off Cape Darnley (Fig.1). During brine rejection, dense shelf water forms (DSW), cools below the freezing point, and freshens from the ice shelf meltwater in the cavity, producing Ice Shelf Water (ISW). The CDBW then flows down Wild Canyon and turns to the west, mixing with CDW or modified Circumpolar Deep Water (mCDW). This process produces the AABW flowing to the West around Antarctica (Mizuta et al., 2024).

https://doi.org/10.5194/egusphere-2025-2515
Preprint. Discussion started: 10 July 2025

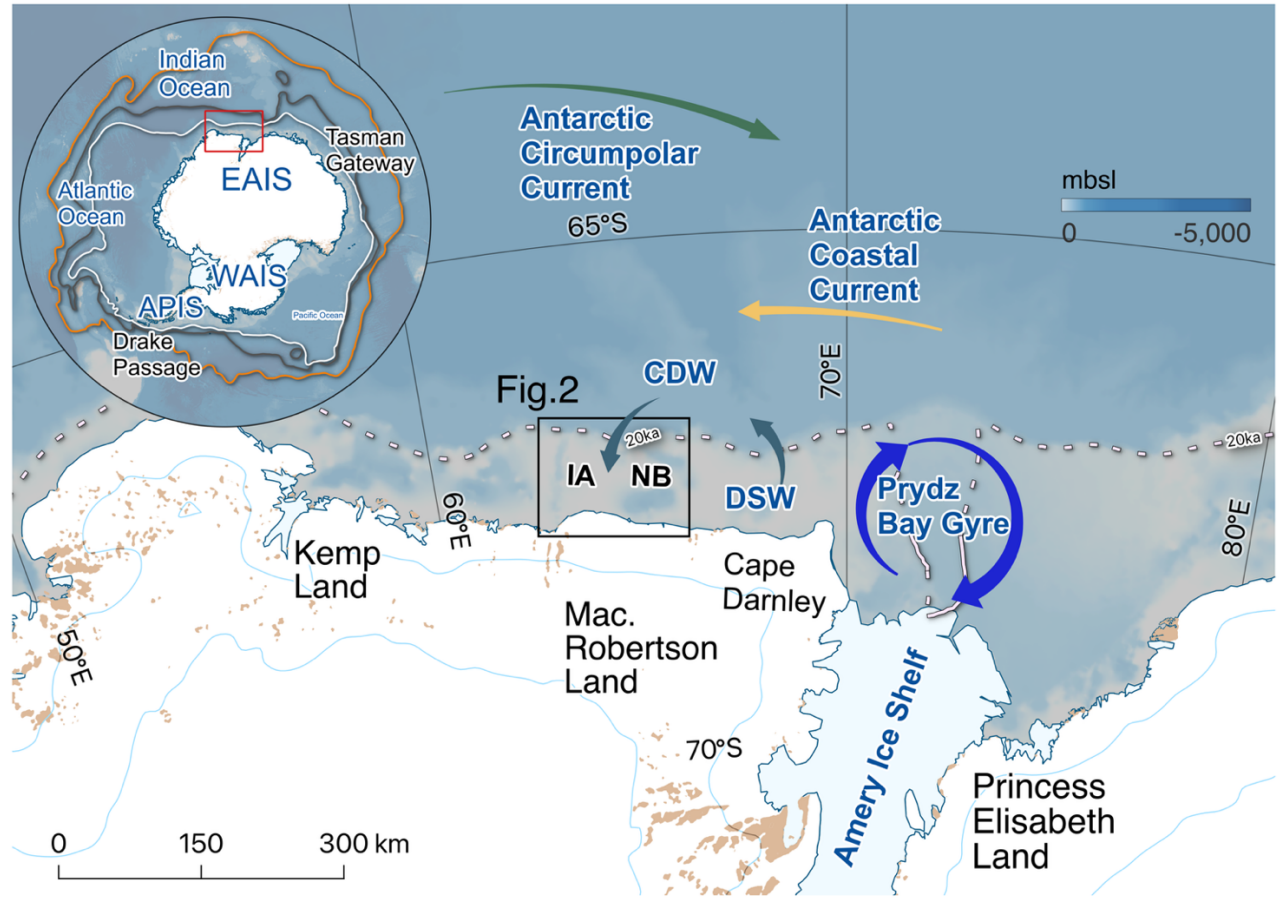

Figure 1: Overview of the broader study area. Orange line (Polar Front), green line (southern ACCF), white line (ACC), and their locations are indicated in the upper left panel. The investigated cores in this study originated from the Nielsen Basin (NB) and Iceberg Alley (IA) on the Mac. Robertson Shelf (black square). The 20 ka dotted line represents the inferred grounding line position at the LGM (The RAISED Consortium, 2014). Arrows indicate the flow direction of the water masses. The basemap has been modified from IBCSO v2 (Dorschel et al., 2022) with Quantarctica QGIS (Matsuoka et al. 2021).

3 Materials and Methods

3.1 Geophysical analyses of the (sub) seafloor

The bathymetric data from PS128 were acquired with the multibeam echosounder (MBES) Teledyne Reson Hydrosweep DS3. The frequency used of the MBES system is ~14 kHz with chirped pulses and is arranged in a Mills Cross configuration of 3 m by 3 m onboard *Polarstern*. At the nadir, the opening angle is 70 ° at both sides. This includes water depths < 2000 m. In greater depths, the angle decreases to ~ 50 ° on each side. The bathymetric data from NBP0101 were acquired with the SEABEAM system (Leventer et al., 2006). Afterward, the data were processed with the standard procedure of the MB-system and gridded to a 50 m x 50 m spatial grid for analysis in QGIS (Dorschel et al., 2022).

https://doi.org/10.5194/egusphere-2025-2515
Preprint. Discussion started: 10 July 2025

Records of sub-bottom profiles were performed using the sub-bottom profiling or sediment echosounding system Teledyne Parasound P70 to image the upper tens of meters of the ocean floor's subsurface. The system generates two primary high-frequency (PHF) acoustic signals in a range of 18-24 kHz. Two secondary frequencies are generated in the water column, of which one is the difference (SLF and one is the sum (SHF). The system's secondary low frequency (SLF) can penetrate the sediment column up to 100 m, depending on the sediment conditions. With the primary high-frequency signal, a higher lateral resolution can be obtained. The primary signals are emitted in a narrow beam of 4.5° and high power, providing a very high lateral resolution (Tiedemann and Müller, 2022). At slopes > 4 °and some rough seafloor topography, the system creates only poor reflections from the seafloor and much less from the sub-bottom. (Klages et al., 2017, Arndt et al. 2017). At the Expedition, the PHF setting was set to 22 kHz and the SLF to 4 kHz. The resulting beam's footprint on the sea bottom is about 7 % of the water depth. The penetration depth in our study area did not reach the full penetration capacity of the system due to the stiffness of the underlying glacial sediments (Tiedemann and Müller, 2022). The correct identification and interpretation of subglacial bedforms crucially depend on the detailed recording of its internal architecture, which can be achieved by acoustic sub-bottom profiling.

3.2 Multi-proxy analyses of sediment cores and dating

A total of eight sediment cores were recovered from the Mac. Robertson Shelf during the RV *Polarstern* cruise "East Antarctic Ice Sheet Instabilities" (AWI 2017; EASI-1; Tiedemann and Müller, 2022) in the Austral summer of 2022. All cores were retrieved with a Kiel-type gravity corer (GC), except PS128_39-1 and PS128_38-2, which were recovered with a piston corer (PC) (see Table 1). The physical properties of each core were measured onboard with a GEOTEK Multi Sensor Core Logger (MSCL). They were then stored at + 4 °C. The visual core description and documentation were performed at the Alfred Wegener Institute (AWI) in Bremerhaven, Germany.

Table 1: Analysed sediment cores for this study. GC: Gravity corer; PC. Piston corer; deg: Decimal degree; mbsl: meters below sea level; mbsf: meters below sea floor; GZW: Grounding-zone wedge.

Core Nr.	Device	Latitude (deg)	Longitude (deg)	Water depth (mbsl)	Core recovery (mbsf)	Location
PS128_45-1	**GC**	-66.952	64.858	356.8	1.29	Outer shelf, Nielsen Basin
PS128_44-1	**GC**	-66.960	64.990	399.8	3.96	Outer shelf, Nielsen Basin
PS128_42-1	**GC**	-67.067	65.498	580.7	4.07	Mid shelf, Nielsen Basin, GZW
PS128_41-1	**GC**	-67.092	65.600	584.4	4.06	Mid shelf, Nielsen Basin, GZW
PS128_39-1	**PC**	-67.115	65.696	660.6	8.60	Mid shelf, Nielsen Basin, sedimentary basin
PS128_38-2	**PC**	-67.142	65.817	524.6	0.77	Mid shelf, Nielsen Basin
PS128_46-1	**GC**	-66.843	63.188	376.1	2.62	Outer shelf, Iceberg Alley, GZW
PS128_47-1	**GC**	-66.828	63.208	389.8	3.92	Outer shelf, Iceberg Alley

https://doi.org/10.5194/egusphere-2025-2515
Preprint. Discussion started: 10 July 2025

The samples were wet-weighed, freeze-dried, ground and dry-weighed for water content and subsequent geochemical analyses, i.e., total organic carbon (TOC) and total nitrogen analyses. The samples were prepared for the TOC measurement by weighing 0.1 g of sediment and removing any inorganic carbon, including carbonates. After decarbonization, the samples were measured with an ELTRA CS800 carbon-sulfur determinator. Standards were measured for calibration to ensure accuracy (error ± 0.02). Bulk sediment C and N contents were obtained with a Vario cube organic elemental analyzer, usually applied to determine the carbon and nitrogen contents of a sample by high-temperature combustion. Blanks and standards were measured for calibration to ensure accuracy (error C, N ± 0,02). The ratio of carbon to nitrogen (C:N) was calculated from TOC/N (%).

The spatula samples were wet-weighed, freeze-dried, dry-weighed, and sieved for grain size classification with a > 2 mm and > 63 µm sieve. The weight percentages were obtained from the dry weight of the sample and the resulting weight of the dried grain size fraction, i.e., gravel (> 2 mm), sand (> 63 µm), and mud (< 63 µm). The water content of each sample has been calculated by subtracting the dry from the wet weight. Smear slides were taken from each identified lithological unit to determine its microfossil content and composition. Sufficient datable material was detected in cores from the outer shelf (PS128_44-1, 45-1, PS128_46-1, and PS128_47-1) and from one mid-shelf core (PS128_39-1) (see Table 2 and Supplements). Dating calcareous microfossils from continental shelf sediments remains challenging due to the scarcity of biogenic carbonate resulting from poor carbonate preservation in sediments bathed in corrosive Southern Ocean deep waters (Hauck et al., 2012). AMS ^{14}C dating was carried out with the MIni CArbon Dating System (MICADAS) on planktic and benthic calcareous microfossils from the sieved sand fraction at the Alfred Wegener Institute, Bremerhaven, Germany, following established workflows. The analysis was conducted on CO_2 gas due to generally small sample sizes (< 2000 µg). The maximum age limit for such sample material has been set to ~42 ^{14}C ka BP (Mollenhauer et al., 2021).

Extracted foraminifer assemblages mainly included the planktic species *Neogloboquadrina pachyderma* in core PS128_45-1 and the benthic species *Globocassidulina subglobosa/biora*, *Cibicidoides spp.* as well as *Ehrenbergina glabra* from the cores PS128_39-1, PS128_44-1, PS128_46-1, and PS128_47-1. For core PS128_39-1, additional Ramped-Pyrolysis-Oxidation (RPO) ^{14}C ages were determined to better constrain the grounding line retreat, because of the lack of foraminifera in the upper part of the core. We used a modified SoliTOC Cube Carbon Analyzer (Elementar Analysensysteme GmbH, Germany), likewise located at the MICADAS. Based on the shape of the thermograms (evolved CO_2 over temperature), the temperature limit for an appropriate fraction was determined such that the upper temperature limit was as low as possible while including a total amount of 80-100 µgC. data (Mollenhauer et al., 2021). A detailed description of the RPO system and the method is given by Kattein et. al. (in preparation, see Supplements Table S1).

Before microfossil extraction from the cores, each sampling depth was closely investigated on x-radiographs to exclude iceberg and/or bioturbation and thus unreliable measurements. The resulting ^{14}C ages have been corrected and calibrated with the Marine20 curve (CALIB 8), carefully considering suggested ΔR values for Holocene samples younger than 11.5 cal. ka before present (BP) and glacial samples older than 11.500 cal.ka BP (Heaton et al., 2024).

https://doi.org/10.5194/egusphere-2025-2515
Preprint. Discussion started: 10 July 2025

4 Results

4.1 Seafloor morphology and sub-seafloor stratigraphy

The allocation in this work in outer, mid, inner shelf is based on general bedform occurrences and transitions as laid out previously in other studies (e.g., Wellner et al., 2006; Graham et al., 2009; Dowdeswell et al., 2016). The interpretation of the identified bedforms can be found in section 5. The mid-shelf submarine glacial landform assemblages can be grouped into three classes: Elongated, streamlined, (sub)parallel features, wedge-like structures, and/or randomly oriented seafloor scours. In Nielsen Basin, a distinct topographic high separates the deeper inner shelf part of the trough from the mid-shelf. This sill has a height of ~550 m. Sea- and landwards of this sill, deeper basins are present. This area is characterized by (sub)parallel, elongated ridges. They tend to appear in clusters with similar orientations and morphometry and elongation ratios >10:1. Towards the top of the sill, they transition into teardrop-shaped features before becoming more elongated again (Fig. 5; b). In Nielsen Basin, mid-shelf teardrop-shaped features mainly occur on the bedrock sill's surface and its lee and stoss sides, respectively. There is an increase in elongation on the lee side of the sill (>20:1). Sub-bottom profiling data indicate a thin out of sediment cover on top of the sill, which thickens inside adjacent basins, containing largely undisturbed layers (Fig.5; b). Toward the outer Nielsen Basin, several wedge-shaped ~1 km long and ~8 m high bathymetric features are located perpendicular to the trough axis, ~35 km and ~41 km away from the continental shelf edge. These features consist of a steep distal and gentle proximal slope. Based on this morphology, their internal composition appears largely transparent to chaotic on the sub-bottom profiles (Fig.5; b). At the mid–outer shelf transition (Fig.5; b, a), the seafloor shallows significantly from ~500 to ~300 mbsl. Here, the sets of elongated, streamlined features become increasingly overprinted by randomly oriented curvilinear structures, which are characterized by a general NNW orientation.

At the outer shelf, the trough widens toward the shelf break. Their distribution comprises the entire outer shelf with highly variable orientations and depths. Most of the scours have an NNW orientation. The orientation changes for some of the scours towards the mid-shelf with an increase in NNE-oriented scours perpendicular to the trough axis. The GZW previously identified by Mackintosh et al. (2011) (Fig.2) has a crest height of ~10 m and a length of ~6 km. Seaward from the GZW, several multidirectional curvilinear features with ~5 to 10 m depths and with up to 200 m widths are preserved.

Similar to the Nielsen Basin, the Iceberg Alley trough is characterized by elongated, streamlined, (sub)parallel features on its inner and mid-shelf part to randomly oriented structures and wedge-like features toward the outer shelf (see Leventer et al., 2006, and Fig.5; c). These features occur in hilly terrain with topographic highs and depressions and can be, similarly to Nielsen Basin, separated into more rounded features at the topographic highs and streamlined forms with a higher elongation ratio towards the outer shelf. Toward the outer shelf, they are replaced by clustered, parallel ridges with high elongation ratios (>16:1) and some deeper ridges with lower parallelism and perpendicular orientation. The outer shelf assemblages resemble the ones identified on the outer Nielsen Basin, including a previously identified GZW and curvilinear and linear iceberg scours

https://doi.org/10.5194/egusphere-2025-2515
Preprint. Discussion started: 10 July 2025

(Fig.2). Here, they show mainly NNE orientations. The GZW lies in water depths of ~ 300 mbsl with a height of ~20 mbsl and a length of 2 km.

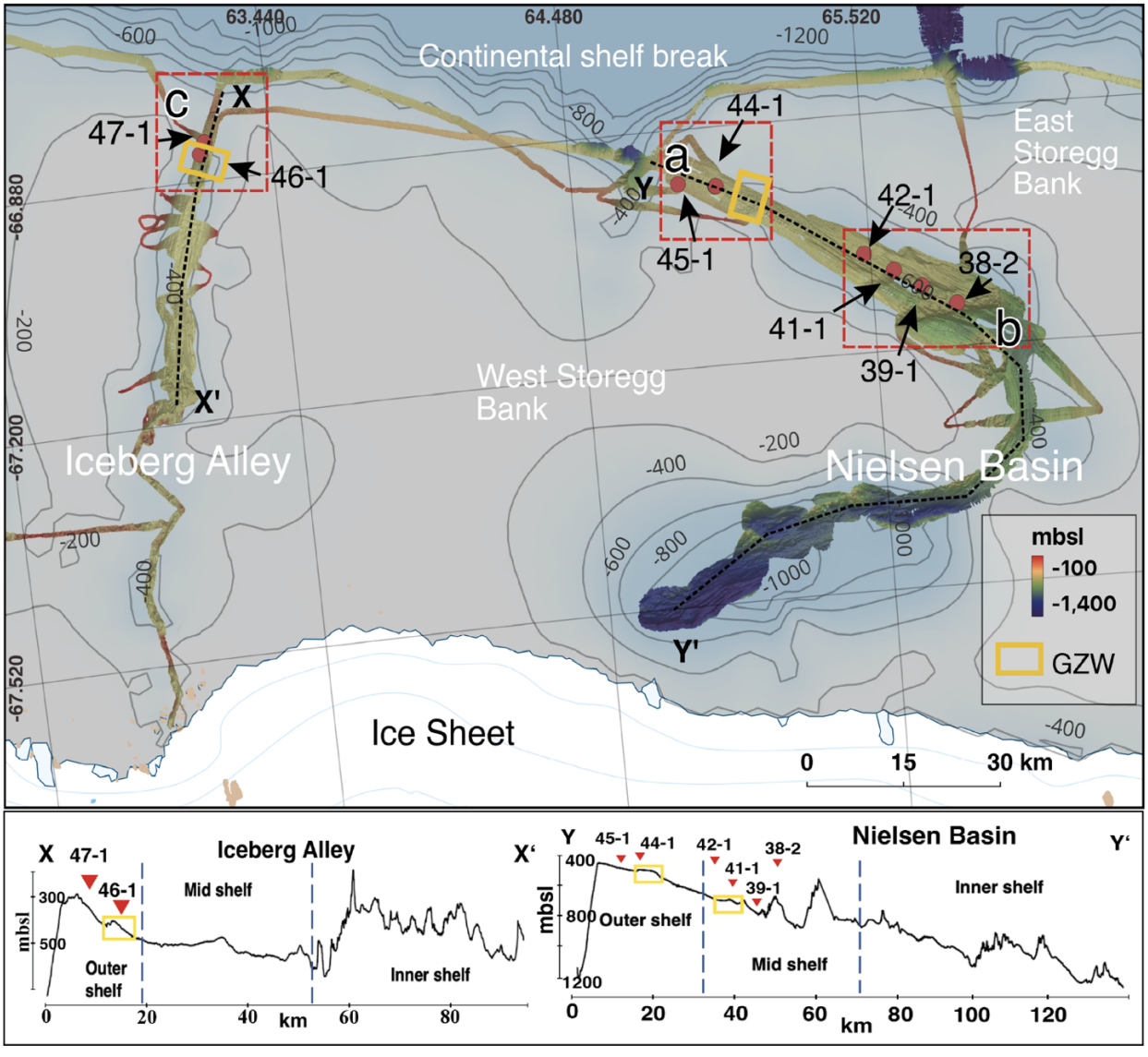

Figure 2: Bathymetric overview of the Mac. Robertson Shelf; coloured depth profile from MBES for NB and IA (PS128/NBP0101). The bottom row shows vertical cross-sections through the IA (left) and NB (right) basin topography. Red dots indicate coring locations (abbreviated for readability), and dashed squares (a-c) zoom-ins are shown in Figure 5. Basemap modified from IBCSO v2 (Dorschel et al., 2022)

https://doi.org/10.5194/egusphere-2025-2515
Preprint. Discussion started: 10 July 2025

4.2 Facies analyses and chronology of sediment cores

For this study, eight gravity cores were recovered from the central mid-outer Nielsen Basin and outer Iceberg Alley (Fig. 1) to explore past grounding line extent and retreat dynamics since the LGM, which we will interpret in the following section and assign them to the different depositional settings (Fig. 3 and 4; see Tables 2-3).

The outer shelf gravity cores PS128_45-1 and 44-1 were retrieved near the continental shelf break, and just landward of the presumed LGM GZW (cf. Mackintosh et al., 2011) (Fig. 2). Mid-shelf cores PS128_42-1 and 41-1 were recovered from the top sets of two GZWs, PS128_39-1 from a sedimentary basin, and PS128_38-2 from a bedrock sill. Gravity cores PS128_46-1 and PS128_47-1 were recovered from the outer shelf in the Iceberg Alley trough (Fig. 2). Here, core PS128_46-1 was taken atop of the presumed LGM GZW (cf. Mackintosh et al., 2011), while PS128_47-1 was located in front of that wedge (Fig. 2, Fig. 5; c).

The outer-shelf cores (PS128_47-1, 45-1, and 44-1) contain massive and consolidated diamictons characterized by high shear strengths and magnetic susceptibilities as well as low water and total organic carbon (TOC) contents without the presence of *in-situ* microfossils (see Fig. 3 and 4 and Supplements Fig. S1). In PS128_46-1, the lowest unit indicates a diamicton-like structure in the CT scans with poorly rounded clasts in a fine matrix. Unlike the unit from the previous cores, they show lower shear strength, medium water content, and high C:N values. Magnetic susceptibility peaks at the base and decreases upwards. From the base to the top, the shear strength in all these cores generally drops, water content increases, magnetic susceptibility fluctuates strongly, and *in-situ* microfossils become more abundant. Additionally, some layers with different-sized clasts of poor angularity are observed in all cores. Some show more prominently stratified layers. Distinct sequences of diatomaceous reddish-brown laminated mud are found in both Iceberg Alley cores (PS128_46-1, 47-1). These sediments are high in mud and low in sand and gravel contents with abundant calcareous and siliceous microfossils (e.g. *Fursenkoina fusiformis, Trifarina* sp., *Cassidulinoides* sp., *Corethron* spp. and *Chaetoceros* spp.).

The lithology toward the top of cores PS128_44-1 and 45-1 revealed fining-upwards sequences followed by coarsening-upwards trends. These sediments are characterized by low shear strength, moderate water and TOC content, and high mud content with decreasing magnetic susceptibility (see Fig. 3 and Supplements Fig. S1). PS128_46-1 and 47-1 are heavily bioturbated and dominantly stratified, likewise abundant in calcareous microfossils (e.g., foraminifera, ostracods, bivalvia, bryozoa).

Proxies measured in the lower part of the two mid-shelf cores (PS128_42-1 and 38-2) resemble the ones from the outer shelf. They consist of massive and consolidated diamictons with high shear strengths and magnetic susceptibilities, low water and TOC contents, and no *in-situ* microfossils.

The shear strength drops at the boundary from the diamicton towards the top of the mid-shelf cores and *in-situ* microfossils get more abundant. The magnetic susceptibility and the atomic C:N ratios indicate strong fluctuations, peaking in the muddy

https://doi.org/10.5194/egusphere-2025-2515
Preprint. Discussion started: 10 July 2025

sand layers of the cores (PS128_41-1, 39-1). There is an increase in biological activity and no pronounced stratification. An increase in clast content is noticed, with some particularly large clasts in core PS128_39-1.

Toward the top of the core, PS128_38-2, 42-1 revealed a fining-upwards sequence followed by coarsening-upwards trends. These sediments were characterized by low shear strength, moderate water and TOC content, and high mud content with decreasing magnetic susceptibility. Microfossils were abundant, including diatoms, radiolaria, and arenaceous foraminifera (e.g. *Miliammina arenacea*), with calcareous foraminifera present in some cores (e.g., *N. pachyderma, Cassidulinoides* sp.). At these depths, PS128_39-1 and 41-1 show very low shear strength, high water and TOC content, and a distinct lithological transition to stratified diatomaceous oozes.

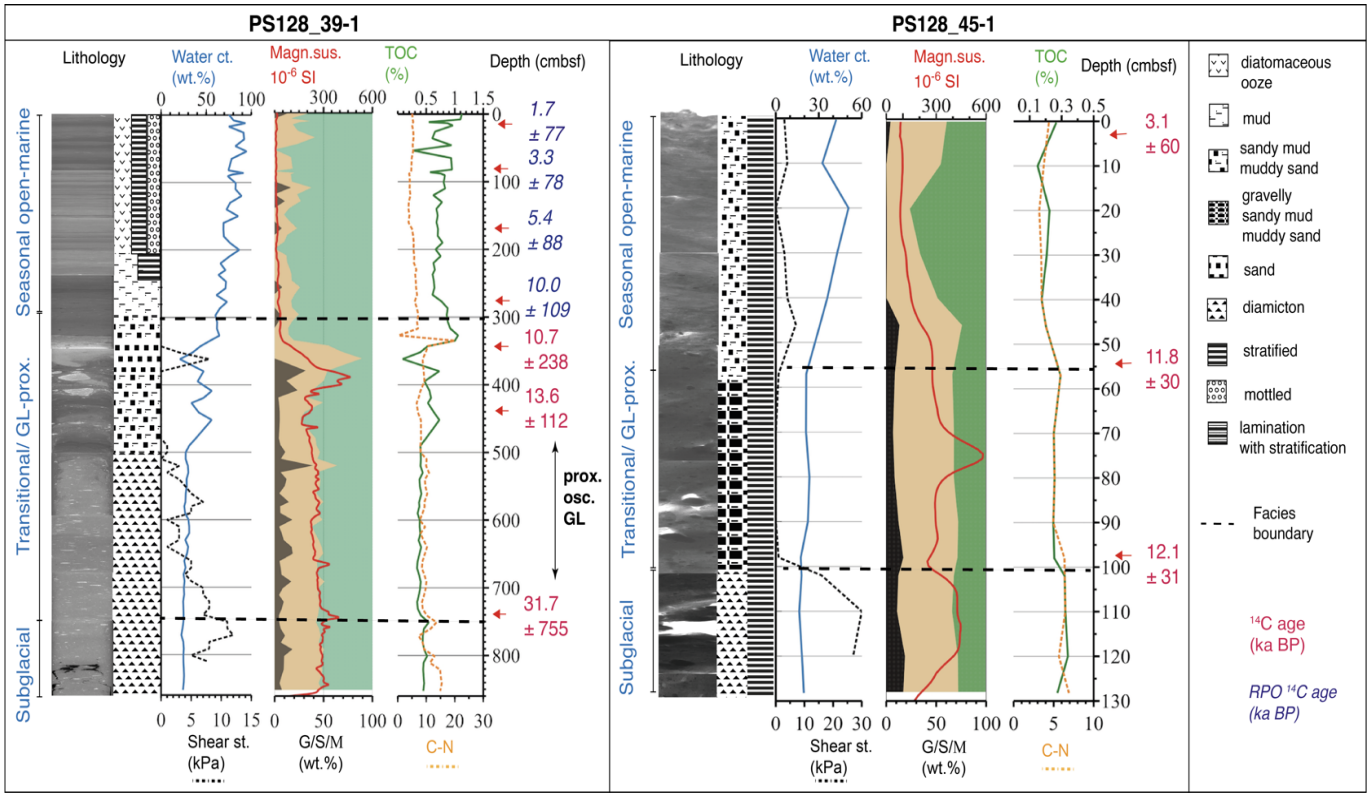

Figure 3: Core parameters of Nielsen Basin mid-shelf core PS128-39-1 and outer shelf core PS128_45-1 (Lithology, Water content wt. %, Shear strength, Grain size distribution wt. %, magnetic susceptibility, TOC %, C:N). Red numbers are uncorrected foraminifer-derived radiocarbon ages. The dashed lines mark the facies boundaries.

https://doi.org/10.5194/egusphere-2025-2515
Preprint. Discussion started: 10 July 2025

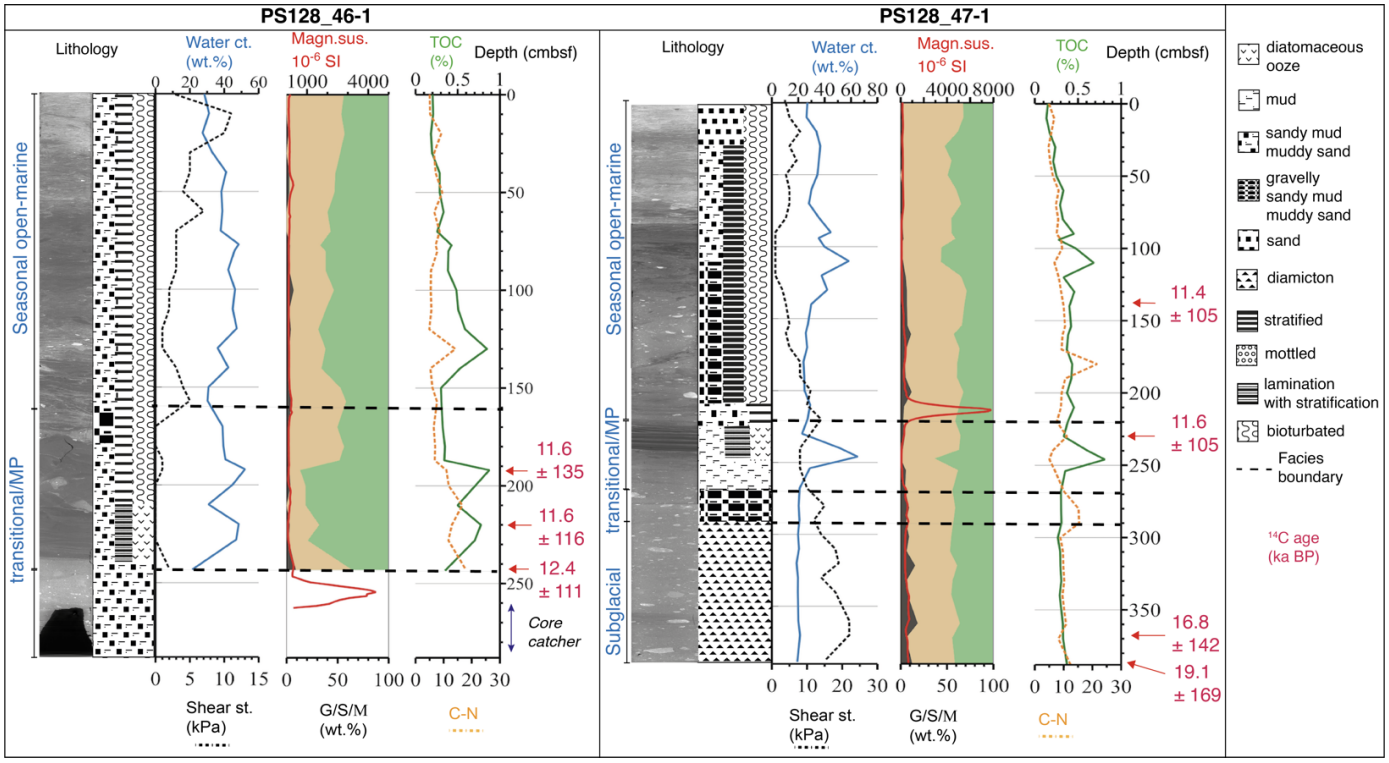

Figure 4: Core parameters of Iceberg Alley shelf cores PS128-46-1 -47-2 (Lithology, Water content wt. %, Shear strength, Grain size distribution wt. %, magnetic susceptibility, TOC %, C:N). Red numbers indicate uncorrected foraminiferal radiocarbon ages. The dashed lines mark the facies boundaries. MP= Meltwater plume facies.

The measured AMS^{14}C dates of the sediment cores PS128_39-1,45-1, 46-1, and 47-1 are listed as conventional ages and calibrated ages in Table 2 and are further discussed in the following section.

Table 2: Conventional and calibrated radiocarbon ages of PS128 and recalibrated JPC40 and JPC43B cores (Heaton et al., 2024). Ages in bold are the minimum age constraints and bold italics are possible maximum ages (carbonate found in subglacial till) used for paleo-grounding line reconstruction. NB = Nielsen Basin, IA = Iceberg Alley, BB=Burton Basin, AIO = Acid insoluble organic matter, RPO=Ramped-pyrolysis-Oxidation

Core Nr./ position	Depth (cmbsf)	Dated material	Conventional radiocarbon ages (^{14}C ka BP) +- error	Calibrated radiocarbon ages Age range (cal. ka BP) 2 sigma rounded	Median (cal. ka BP) rounded
PS128_39-1	**352**	Benthic foraminifera	**10,719 +-238**	**10,300-11,700**	**11,000**
Mid shelf basin	452	Benthic foraminifera	13,150 +-112	13,300-13,900	13,600
NB	741	Benthic foraminifera	31,731 +-755	32,800-36,100	***34,500***

https://doi.org/10.5194/egusphere-2025-2515
Preprint. Discussion started: 10 July 2025

RPO ages PS128_39-1					
286°C	4.5	Bulk sediment	1,708+-75	310-650	500
294°C	79.5	Bulk sediment	3,381+-78	2,000-2,500	2,300
293°C	178.5	Bulk sediment	5,464+-88	4,700-5,200	5,000
287°C	284.5	Bulk sediment	10,010+-109	9,700-10,300	**10,000**
294°C	338.5	Bulk sediment	11,571+-173	11,300-12,400	11,800
283°C	348.5	Bulk sediment	11,990+-177	11,900-12,800	12,400
PS128_45-1	1	Planktic foraminifera	3,153 +- 60	1,800 – 2,200	2,000
Outer shelf	57	Benthic foraminifera	11,802 +-30	12,000 – 12,400	12,200
NB	98	Benthic foraminifera	**12,169 +-31**	**12,500 - 12,700**	**12,600**
PS128_47-1	140	Benthic foraminifera	11,454 +-105	11,700-12,400	12,100
Outer shelf	230	Benthic foraminifera	**11,669 +-105**	**12,000-12,600**	**12,300**
IA	268	Benthic foraminifera	39,619 +-920	40,700-42,900	41,900
	280	Benthic foraminifera	26,270 +-279	28,000-29,300	***28,700***
	370	Benthic foraminifera	16,896 +- 142	18,100-18,800	18,500
	388	Benthic foraminifera	19,192 +-169	20,700-21,700	21,200
Recalibrated radiocarbon ages from Leventer et al. 2006					
JPC40-NB					
Mid shelf	**2141**	AIO	**13,520**	**13,700- 14,600**	**14,100**
JPC43B-IA					
Mid to outer shelf	2310-2315	AIO	**11,770**	**12,300- 12,700**	**12,500**
PS69/849-2-BB (Borchers et al., 2016)					
Mid shelf	275	AIO	**12,030 +-90**	**12,200-12,700**	**12,500**

5 Interpretation

5.1 Seafloor geomorphology

265 The elongated, streamlined and parallel bedform assemblages identified on the Nielsen Basin mid-shelf clearly resemble mega-scale glacial lineations (MSGL) identified on other Antarctic continental shelves (e.g., King et al., 2009). They usually form under wet-based, fast-flowing ice streams on soft, deformable substrates such as glacial tills as a result of till deformation and

https://doi.org/10.5194/egusphere-2025-2515
Preprint. Discussion started: 10 July 2025

basal sliding, often underlain by a consolidated, stiff till (e.g.,Reinardy et al., 2011). Different sets of N-NNW-oriented MSGLs within the curved trough (Fig. 5; b) may imply their multi-temporal formation (e.g., Graham et al. 2009). They show an increase in elongation on the lee side of the bathymetric sill. Usually, this is associated with flow acceleration at substrate boundaries and deforming bed conditions (Graham et al., 2009). We furthermore interpret the teardrop-shaped features on the mid-shelf as 'drumlinoid features'. They are associated with ice-flow deceleration (e.g., Graham et al., 2009). They often, as on top of the Nielsen Basin bedrock sill (Fig.5; b), comprise roche moutonneés, whalebacks, and/or crag-and-tail structures (Fig.5; b). Variations in sizes and shapes result from differences in local substrates, changing ice flow conditions or small-scale variations in basal conditions (Graham et al. 2009).

The wedge-like features on the Nielsen Basin mid to outer shelf transition are identified as grounding-zone wedges (GZWs), closely resembling numerous features previously reported from Antarctic continental shelves (e.g., Jakobsson et al., 2011; Klages et al., 2014, 2015, 2017; Batchelor and Dowdeswell, 2015). GZWs dimensions are controlled by sediment delivery, duration of stillstand, cavity shape, and the width of the streaming ice margin (e.g., Dowdeswell and Fugelli, 2012). They co-occur on the mid-outer shelf boundary with linear to curvilinear iceberg scours formed by the seafloor-scouring keels of grounded icebergs (e.g., Dowdeswell and Hogan, 2016). They are usually associated with a calving ice shelf or seasonal open marine conditions in water depths shallower than iceberg keel draughts (e.g., Dowdeswell et al., 2016). On the outer shelf toward the shelf break, the curvilinear features also belong to the bedform assemblage of iceberg scours (Klages et al., 2015, 2017).

Seaward from the previously described GZW, several multidirectional curvilinear scours are present. They likely result from the transition of a grounded or sub-ice shelf environment where ice reaches flotation in newly opened ice shelf cavities, producing deeper scours in shallower water depths (Smith et al., 2019). Beyond the shelf break, the presence of gullies indicates a GL position at or close to the shelf break, which bulldozed glacial debris and discharging sediment-laden meltwater plumes into the channels leading to debris flows and turbidity currents towards slope and rise (e.g., Lowe and Anderson 2002).

In Iceberg Alley, the streamlined subparallel features from the inner to mid shelf were likewise classified as 'drumlinoid features'. They likely formed under similar circumstances as in Nielsen Basin from differences in local substrate underneath the streaming ice. On the outer shelf, we identified these clustered parallel ridges as MSGL and some deeper ridges with low parallelism as iceberg scours. Some of them are cross-cutting (Fig.2), indicating the presence of large, multidirectional icebergs that were calving close to the ice sheet margin at different timescales. The previously identified GZW on the Iceberg Alley outer shelf is superimposed on the MSGLs and, therefore, suggests an earlier formation of the MSGLs.

https://doi.org/10.5194/egusphere-2025-2515
Preprint. Discussion started: 10 July 2025

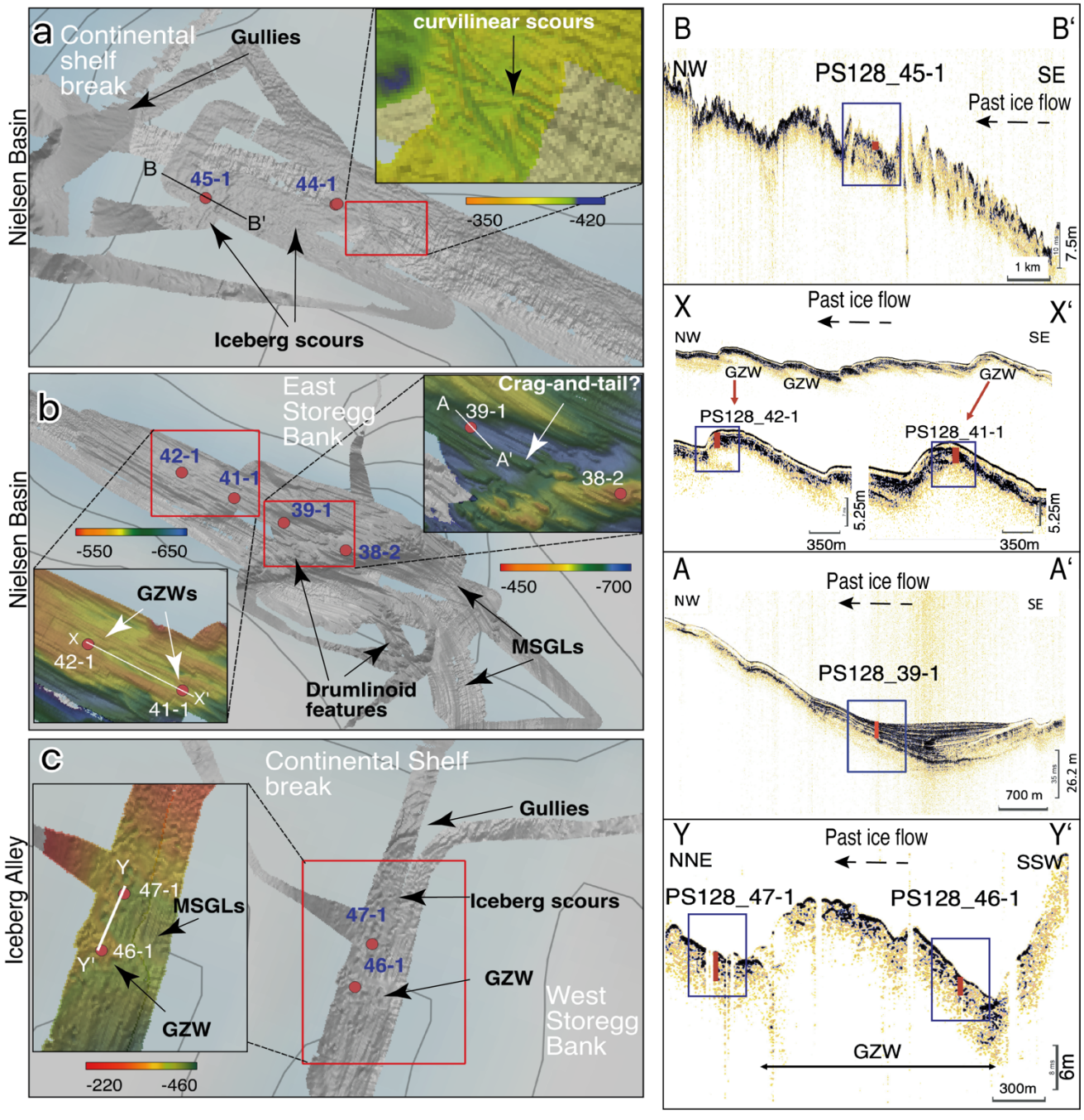

Figure 5: Bathymetric map of the outer (a, c) and middle shelf (b) in Nielsen Basin and Iceberg Alley. Red dots indicate coring locations from figure 2 (abbreviated for readability). The PARASOUND profiles across outer shelf Iceberg Alley (Y-Y'), mid-shelf GZWs Nielsen Basin (X-X'), outer shelf GZW Nielsen Basin (B-B') and across sediment basin seaward the bedrock sill (A-A') with coring locations indicated. The sub-bottom profiles reveal internal structures of the GZWs. Isobaths plotted from IBSCO v2 (Dorschel et al., 2022.)

https://doi.org/10.5194/egusphere-2025-2515
Preprint. Discussion started: 10 July 2025

5.2 Sedimentary facies and depositional environments

The geological record of grounding line retreat in gravity cores from the Antarctic continental shelf is usually evident from three to four sedimentary facies reflecting the changing conditions at a particular site from subglacial over grounding line-proximal and sub-ice shelf to open-marine deposits (e.g., Hillenbrand et al., 2014; Klages et al., 2013). Ideally, such facies successions can be put into chronological context by dating *in-situ* calcareous microfossils or – if the sedimentary environment allows (Hillenbrand et al., 2010) – bulk organic carbon. The assigned depositional setting for the lithological units and measured proxy values are listed in Table 3.

The proxies from the lowest lithological unit of the outer shelf cores PS128_47-1, 45-1, and 44-1 show characteristic signatures of glacially deposited sediments (refer to section 4.2). Based on these characteristics, we interpret these sediments as a subglacial till deposited beneath an ice sheet (e.g., Hillenbrand et al., 2014, Klages et al., 2013). The contained clastic grains in this unit are mostly metamorphic, hence indicating a subglacial terrigenous supply from the hinterland (eg. Mackintosh et al., 2007). In core PS128_46-1, a marine-influenced grounding line-proximal deposition is present at the bottom of the core because the gravity corer did not reach the subglacial till.

The increase in water content with a decrease in sediment compaction and higher biological activity towards the top in all of these cores indicates the onset of a retreating grounding line. The metamorphic clasts found in these units likely result from sub-ice shelf rain-out and iceberg calving, and are classified as IRD, suggesting sub-ice shelf environments. We interpret this facies as a transitional or grounding line-proximal facies (see Fig.3 and 4). In PS128_44-1, the transitional facies is characterized by proxy signatures indicative of an ice-shelf break-up with iceberg turbates, resulting from calving at an ice front. The microfossils found in the transitional zone of cores PS128_46-1 and 47-1 are presumed to indicate seasonal phytoplankton blooms due to iron-rich meltwater input from iceberg calving (Sedwick et al., 2001; Alley et al., 2018). Majewski et al. (2020) assigned these specimens of foraminifera as indicative of a meltwater plume or proximal glaciomarine environment.

The proxies of the lowest unit of the mid-shelf Nielsen Basin cores PS128_42-1 and 38-2 are characterized by a highly compacted, unsorted sediment with dispersed clasts and low organic matter (refer to section 4.2). We assigned these to a subglacial till (see Supplements Fig. S1). The cores PS128_41-1 and 39-1 show similar characteristics but with higher variability. This suggests a mixed input from terrestrial and marine sources with low biological activity, suggesting permanent ice-shelf cover proximal to the grounding line. We interpret this as a grounding line-proximal facies (refer to section 4.2, Fig. 3 and Supplements S1). Toward the top of the cores PS128_41-1 and 39-1, the proxies indicate a transitional or grounding line-proximal facies with basal melt-out and calving of icebergs from the ice shelf. We identified the large clasts found in the

https://doi.org/10.5194/egusphere-2025-2515
Preprint. Discussion started: 10 July 2025

transitional zone of core PS128_39-1 as dropstones, either from the calving front of an ice sheet or sub-ice shelf rain-out very close to the grounding line from the ice sheet's base. The proxies of the top unit in these cores indicate an open marine deposition with seasonal peaks of phytoplankton blooms during sea-ice-free periods. Abundant microfossils and the absence of IRD suggest an already advanced grounding line retreat toward the inner shelf from this position.

Table 3: Summary table of characteristic lithofacies with assigned depositional settings (ST=shear strength, water ct.=water content wt. %, MS=magnetic susceptibility, TOC=total organic carbon, GL=grounding line, IRD= ice-rafted debris).

Lithofacies/ Structure	Parameters	Interpreted depositional setting and processes
Diamicton massive	High ST (>10 kPa), medium to low water ct., high uniformly distributed MS, TOC < 0.5, medium C:N, metamorph, crystalline gravels	Massive ice-contact sediment with unsorted and poorly rounded crystalline gravel in a fine matrix. Highly compacted sediment with no in-situ to sparce reworked poorly preserved microfossils: **Subglacial till**
Diamicton stratified	Low to medium ST (<10 kPa), Water ct. < 40, High MS, TOC < 0.7, Low to medium C:N, metamorph crystalline gravels	Stratified ice-contact sediment with crystalline gravel in a fine matrix, some microfossils and less compacted sediment: **GL proximal/ sub-ice shelf diamicton/ waterlain till**
Gravelly muddy sand stratified	Medium ST (5-10 kPa), Water ct. < 60, High MS, TOC < 0.6, Medium C:N, high clast content, increasing amout of larger sized clasts	High clast content from icebergs (IRD) or rain-out from basal ice shelf, high microfossil content: **Sub-ice shelf close to calving line / seasonal open-marine close to calving line**
Sandy mud stratified	Low ST (<5kPa), Water ct. 25-50, Moderate MS, TOC < 0.7, Medium C:N, Low clast content	Hemipelagic deposition with high microfossil content sometimes alternating settling of diatom-bearing sediments: **Sub-sea ice to seasonal open-marine**
Muddy sand stratified and non-stratified	Low to medium ST (<10 kPa), Low to medium water ct., Low MS, TOC< 1.0, high C:N, low clast content	Hemipelagic deposition sometimes stratified or bioturbated: Fine-grained hemipelagic sediments, high microfossils (planktic foraminifera), clasts from sub-ice shelf melt-out or calving: **Sub-sea ice to seasonal open-marine**
Mud stratified	Low ST (< 5 kPa), Water ct. > 50, Low MS, TOC > 0.6, Low C:N No clasts	Fine-grained hemipelagic sediments, high microfossils (planktic foraminifera) and organic matter content, few IRD probably melt-out from sea-ice: **Seasonal open-marine**
Mud Diatom-bearing mottled	Low to medium ST (<10 kPa), Water ct. > 50, Low MS, TOC > 0.5, Low C:N No clasts	Alternating settling of glaciomarine hemipelagic and meltwater plume material, high microfossil content: **Sub-sea ice to Seasonal open-marine, meltwater induced**
Diatomaceous ooze mottled stratified	Low ST (0 kPa), Water ct. > 60, Low MS, TOC > 0.7, Low C:N No clasts	Alternating settling of pelagic material indicating annual phytoplankton blooming events, high abundance in diatoms: **Seasonal open-marine**

https://doi.org/10.5194/egusphere-2025-2515
Preprint. Discussion started: 10 July 2025

Our radiocarbon dating at the transition from the subglacial till to the transitional facies in core PS128_45-1 suggests a retreat at ~12.5 cal. ka BP from the Nielsen Basin outer shelf. The transition from subglacial till to glaciomarine deposits in core PS128_47-1 reveals ages around ~12.3 cal. ka BP, suggesting a similar retreat age in Iceberg Alley. Core PS128_39-1 indicates GL oscillations around ~13.6 cal. ka BP, while the boundary to the transitional facies in PS128_39-1 is dated with ~11.0 cal. ka BP, marking the onset of the Holocene (see Table 2). The RPO ages for the upper ~350 cm of the core range from 12.4 cal. ka BP to 10.0 cal. ka BP for the sandy and the sandy mud lithological unit of the transitional facies over an AMS age range of 5.0 cal. ka BP to 0.5 cal. ka BP towards the top of the core for the diatomaceous oozes (Table 2). Here, the sedimentation changes from a lower to a higher sedimentation rate, which is characteristic of deglacial sediments. These ages underline the assumption of a GL retreat somewhere between 11.0 and 10.0 cal. ka BP and the onset of the diatomaceous oozes with seasonal open-marine conditions around the start of the Holocene.

6 Discussion

6.1 Maximum extent and episodic grounding line retreat since the LGM

Previous studies from around the Antarctic continental shelf suggest a grounded ice sheet at or close to the continental shelf break at the LGM (e.g. Anderson et al., 2014; Hillenbrand et al.,2014; Hodgson et al., 2014; Larter et al., 2014; Mackintosh et al., 2014; Ó Cofaigh et al., 2014; Klages et al., 2014, 2015, 2017). Only few studies investigated the ice sheet retreat since the last glacial termination. These studies revealed characteristic glacial facies in the outer Nielsen Basin as well as prominent deglacial deposits of alternating varves of iron-rich sediments and diatomaceous oozes in cores from both inner shelves (Harris and 0'Brien 1998; Leventer et al. 2006). Channel systems on the upper slope of the Mac. Robertson Shelf suggests GL-advance towards the shelf break, bulldozing sediment down the shelf break during ice advances at some point in the past. Our multi-proxy dataset indicates that grounding lines of fast-flowing ice streams within Nielsen Basin and Iceberg Alley reached the shelf break prior to ~12.5 cal. ka BP (Table 2, Fig.5).

Our foraminiferal age from the boundary between the GL-proximal diamicton and the transitional facies indicates a minimum retreat of the GL around ~12.5 cal. ka BP further from the outer shelf towards the mid-shelf in both basins. We assume a formation of the outer shelf GZWs during that period. This implies that they did not form during the LGM and are post-LGM features. MSGLs indicate fast-streaming wet-based ice before the GZW formation. Thus, we propose a nearly synchronous initial retreat of the GL from the outer shelf in both glacial troughs (Fig.6). A lateral narrowing of the trough might have slowed down ice retreat due to lateral pinning on the shallower banks on each side of the trough. After the lateral pinning of the ice sheet, conditions favored GZW formation. This supports the hypothesis that lateral and vertical bathymetric pinning points are important factors slowing down ice retreat (Batchelor and Dowdeswell, 2015). The iceberg scours and furrows identified on the Nielsen Basin outer shelf reveal different orientations and depths and overprint each other at some locations. This indicates that they were likely produced during several calving events of different stages of ice retreat in varying water depths. Multiple

https://doi.org/10.5194/egusphere-2025-2515
Preprint. Discussion started: 10 July 2025

generations of keel scours have been documented on the outer shelf. The older scours exhibit no orientation and are, therefore, probably caused by calving at an ice front. The younger scours are interpreted to be of Holocene age, due to a westward orientation implicating a drift caused by outer shelf currents without lateral constraints by ice bodies (Harris and O'Brien, 1998; Leventer et al., 2006). Both troughs significantly deepen into retrograde slopes at the transition from the outer to the mid-shelf. Here, MSGLs are abundant, indicating a fast-flowing ice stream at the time of formation. The grounding line retreat likely accelerated at this part of the basin, possibly resulting from enhanced CDW inflow into the newly formed ice shelf cavity caused by augmented freshwater inflow from melting at the ice shelf base. In Nielsen Basin, several stabilization events occurred during GL retreat on the mid-shelf. The small size and close spacing of the identified GZWs point toward a short ice sheet stabilization at the boundary from the outer shelf to the mid-shelf. The mid-shelf GZWs are likely deposited after ice sheet pinning to outcropping bedrock.

The AIO radiocarbon ages from core JPC40 (Leventer et al., 2006) indicate a deglaciation of ~14.1 cal. ka BP for the mid-shelf. Yet, comparisons between AIO and foraminiferal ^{14}C ages need to be treated tentatively, because AIO dates often are affected by contamination, resulting in older AMS ages with a drastic down-core increase of ^{14}C ages. We attribute the older radiocarbon ages to entrained carbon in the bulk samples, leading to a modified deglaciation age. However, we cannot rule out the possibility that the outer shelf deglaciation started earlier, between 13.0 and 14.0 cal. ka BP. The additional RPO ages in core PS128_39-1 help to better constrain the onset of deglaciation for Nielsen Basin mid-shelf. Here, the facies association of the different lithological units and reworking of carbonate material proximal to the retreating GL complicate to constrain the exact timing. A bigger offset of the ages at the depths of ~350 to 330 cmbsf can be explained by increased biological activity at this interval, manifested through bioturbation marks. The ages above 330 cmbsf indicate the onset of the Holocene. This strengthens the foraminiferal ages retrieved at this interval.

AIO radiocarbon dates of the Iceberg Alley at the boundary from the outer to the mid-shelf reveal an age of ~12.6 cal. ka BP for the deglaciation (Leventer et al., 2006). Borchers et al. (2016) propose a similar AIO deglaciation age (~12.5 cal. ka BP) for the mid-shelf of the East from Nielsen Basin situated Burton Basin. This strengthens the assumption of a nearly synchronous grounding line retreat across the Mac. Robertson Shelf. Foraminiferal ^{14}C ages retrieved from some sparse specimens (*Globocassidulina sp.*) in the GL proximal and subglacial till indicate an age of ~28.7 cal. ka BP (Iceberg Alley) and ~34.5 cal. ka BP (Nielsen Basin). We cautiously propose this as a maximum glaciation age from older entrained microfossils in the subglacial till.

https://doi.org/10.5194/egusphere-2025-2515
Preprint. Discussion started: 10 July 2025

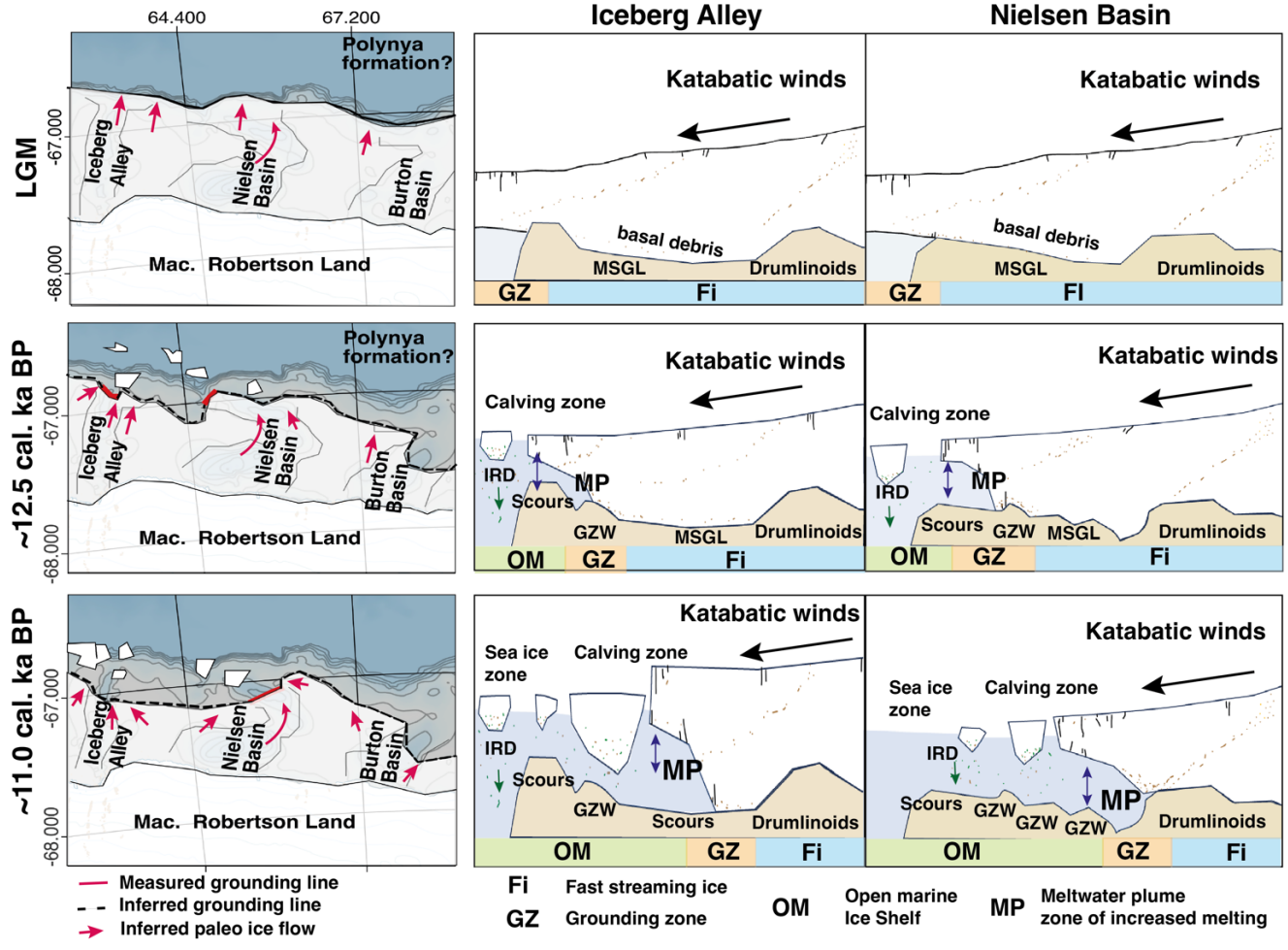

Figure 6: Conceptual model of grounding line extent and retreat on the Mac. Robertson Shelf for the LGM to before ~12.5 cal. ka BP, ~12.5 to before ~11.0 cal. ka BP and shortly after ~11.0 cal. ka BP. The ice sheet's grounding line extent is illustrated on the continental shelf for the three main basins (left) with measured paleo-grounding line (red) and inferred grounding line on adjacent inter-ice stream ridges (dashed black line). Red arrows indicate reconstructed ice flow directions inferred from basin topography and bedform orientation. The vertical cross-section through Iceberg Alley (IA) and Nielsen Basin (NB) are illustrated (right) based on facies analysis of sediment cores, radiocarbon ages and glacial bedforms (schematic representation; not to scale).

6.2 Wider context of Mac. Robertson Shelf deglaciation and relevance for AABW formation

The deglaciation of the Mac. Robertson Shelf at ~12.5 cal. ka BP coincides with the end of the ACR, a temporary atmospheric and oceanic cooling in the Southwest Pacific due to deglacial changes in the Atlantic Meridional overturning circulation, while a warming occurred in the Northern hemisphere (Eaves et al. 2024). It lasted from ~ 14.5 to ~13.0 ka BP (Pedro et al., 2016). Our deglaciation ages reveal an onset too late (after 14.2 ka BP) for being assigned to MWP-1a. Thus, elevated meltwater

https://doi.org/10.5194/egusphere-2025-2515
Preprint. Discussion started: 10 July 2025

discharge and the disintegration of large parts of the ice sheet might have been triggered by the sea-level rise at the MWP-1b between 11.5 and 11.2 ka BP and enforced intrusion of warmer mCDW onto the shelf. Deglaciation ages are sparse for East Antarctic continental shelves, but compared to measured deglaciation ages of Prydz Bay, the Mac. Robertson Shelf stayed glaciated for a much longer time. In Prydz Bay, the continental shelf break was ice-free at the LGM, with much earlier deglaciation in the inner Prydz Channel at the Amery Ice Shelf prior to the LGM that did not reach the continental shelf break (Domack et al.,1998; Hemer and Harris 2003; Guitard et al., 2016). Along the Antarctic Peninsula, the initial retreat was finalized by 18.0 cal. ka BP. In West Antarctica, the GL underwent a substantial retreat from the outer shelf prior to 15.0 cal. ka BP (The RAISED Consortium., 2014). Because GL retreat around Antarctica results from several driving forces such as oceanic conditions, bathymetry, prior ice extent, and ice sheet thickness, as well as bottom substrate composition, the overall ice sheet retreat varies widely between the regions. For example, the West Antarctic continental shelf is characterized by widespread retrograde slopes towards the coast. Controversially, this is less pronounced on the East Antarctic continental shelf, except for cross-shelf glacial troughs (Morlinghem et al., 2020). This implies to restricted mCDW pathways onto the shelf. Another influencing factor for the intensity of mCDW shelf intrusions is the composition of the water column and their prevailing currents at the continental shelf break. Cosmogenic exposure ages from other East Antarctic regions, such as the shelf area of Lützow-Holm Bay in Eastern Dronning Maud Land, also indicate a retreat coinciding with the intrusion of mCDW (Kawamata et al, 2020). Isopycnals, stratified density layers of the ocean, at the shelf break influence which water masses can access or ventilate the shelf. Thompson et al. (2018) classified the East Antarctic area around the Mac. Robertson Shelf as a 'dense shelf' regime. This oceanic regime is characterized by persistent strong easterly winds and a westward-flowing Antarctic Slope Current. Here, strong fronts separate cold and fresh shelf water from warm and salty CDW offshore, leading to a weak cross-slope exchange of water masses. In this regime, it is much harder for mCDW to intrude onto the shelf compared to a 'warm shelf' regime, which prevails around most of West Antarctic continental shelves (Thompson et al., 2018). All of the above may have led to a more resilient ice sheet, delaying grounding line retreat on the Mac. Robertson Shelf. A fully glaciated continental shelf during the LGM would imply a shut-off of AABW or point towards a different formation area from polynyas beyond the continental shelf break further offshore.

Future studies need to focus on the forcings of the grounding line retreat and advanced data of outer shelf deglaciation from adjacent areas along the East Antarctic Indian and Atlantic margin to connect grounding line retreat patterns. This is essential for assessing the broader impact of ice-ocean-atmosphere interactions throughout the last glacial period. Additionally, temperature reconstructions for tracing past CDW intrusions would be beneficial. Volume estimations of past ice sheets on the East Antarctic shelves by combining terrestrial cosmogenic exposure dates with marine radiocarbon measurements might complete the overall picture of past ice sheet dynamics.

https://doi.org/10.5194/egusphere-2025-2515
Preprint. Discussion started: 10 July 2025

7 Conclusion

Our study is the first to combine a multi-proxy approach of geochemical, geophysical, and sedimentological data for a transect through the Nielsen Basin. Thus, it provides new insights into ice sheet grounding line dynamics on the Mac. Robertson Shelf, including the timing determined from AMS ^{14}C ages, exclusively from foraminiferal carbonate. This allows the creation of reliable spatiotemporal benchmarks for ice sheet simulations for the Nielsen Basin. Further, it allows a reliable determination of the grounding line retreat from the outer shelf in Iceberg Alley. We conclude the presence of a wet-based fast-flowing ice stream and episodic ice sheet retreat with several stabilization phases for both troughs from the LGM to today. Furthermore, the radiocarbon ages of core PS128_45-1 and PS128_47-1 contradict a presumed LGM age of both previously identified GZW on the Mac. Robertson Shelf, leading to the assumption of a grounded ice sheet at the Mac. Robertson Shelf break during the LGM. This would have prevented DSW formation at the Cape Darnley Polynya and, thus, AABW formation. This results in either a shutdown of AABW or another formation area off the continental shelf.

Further investigations may focus on the forcings of the grounding line retreat in the region, such as temperature reconstructions for tracing past CDW intrusions. This would be beneficial for assessing broader impacts of ice-ocean-atmosphere interactions throughout the last glacial cycle.

Data availability The metadata of sediment cores and multibeam bathymetric data presented here will be available later at the PANGAEA data repository (https://doi.pangaea.de/10.1594/PANGAEA.982379). Temporary reviewer access key available.

Supplements

Figure S1**:** Core parameters of Nielsen Basin cores PS128_38-2, 41-1,42-1 and 44-1 (CT, Lithology, Shear strength, Water ct., Corg, C:N, Grain size)

Table S1: Full list of all measured conventional and calibrated radiocarbon ages and full description of Ramped Pyrolysis Oxidation (RPO).

Author contribution J.G. participated in conceptualizing, data sampling, data analysis and interpretation, as well as visualization and writing of the manuscript. J.M. was involved in expedition planning, core recovery and data analysis. R.T. was involved in expedition planning and core recovery. G.M. was involved in core recovery and the radiocarbon analysis. L.L-J. was involved in core recovery and data analysis. E.W. was responsible for the PARASOUND data collection and visualization. L.S and N.W. participated partly in data analysis. L.K. participated in the radiocarbon analysis. A.M. was involved in cruise planning and data discussion. J.P.K. was responsible for conceptualization, cruise planning, core recovery, supervision, data collection and analysis and interpretation. All authors took part in the discussion of the manuscript. All authors read the manuscript, commented on the submitted version and agreed to its submission.

Competing interests The authors declare that they have no conflict of interest.

Acknowledgements We thank the captain and crew of RV *Polarstern* Expedition PS128 “EASI-1” (Grant Number PS128_00) as well as V.Schumacher, P.Daub, H.Roeben, Y.Schulze-Tenberge and M. Seebeck for their diligent help on board and in the

https://doi.org/10.5194/egusphere-2025-2515
Preprint. Discussion started: 10 July 2025

lab. C.Gebhardt and T.Bozkuyu for the processing of the MSCL data and F. Nitsche for providing the NBP0101 bathymetric grids.

Financial support J.G. has been supported by the International Science Program for Integrative Research in Earth Systems (INSPIRES IV) at the Alfred Wegener Institute, Helmholtz Centre for Polar and Marine Research. J.M., R.T., L.L.-J., G.M., E.W., J.P.K. were funded by the Helmholtz Association's Research Program "Changing Earth–Sustaining our Future". L.K. received support from the International Science Program for Integrative Research in Earth Systems (INSPIRES III) at the Alfred Wegener Institute, Helmholtz Centre for Polar and Marine Research. A.M. was supported by the Australian Research Council (ARC) SRIEAS grant SR200100005, Securing Antarctica's Environmental Future.

References

Alfred-Wegener-Institut Helmholtz-Zentrum für Polar- und Meeresforschung (AWI).: Polar Research and Supply Vessel Polarstern Operated by the Alfred-Wegener-Institute. Journal of large-scale research facilities, 3, A119. http://dx.doi.org/10.17815/jlsrf-3-163. 2017.

Alley, K., Patacca, K., Pike, J., Dunbar, R., and Leventer, A.: Iceberg Alley, East Antarctic Margin: Continuously laminated diatomaceous sediments from the late Holocene, Mar. Micropaleontol. , 140, 56–68, https://doi.org/10.1016/j.marmicro.2017.12.002, 2018.

Anderson, J. B., Conway, H., Bart, P. J., Witus, A. E., Greenwood, S. L., McKay, R. M., Hall, B. L., Ackert, R. P., Licht, K., Jakobsson, M., and Stone, J. O.: Ross Sea paleo-ice sheet drainage and deglacial history during and since the LGM, QSR, 100, 31–54, https://doi.org/10.1016/j.quascirev.2013.08.020, 2014.

Arndt, J. E., Hillenbrand, C.-D., Grobe, H., Kuhn, G., and Wacker, L.: Evidence for a dynamic grounding line in outer Filchner Trough, Antarctica, until the early Holocene, Geol., 45, 1035–1038, https://doi.org/10.1130/G39398.1, 2017.

Batchelor, C. L. and Dowdeswell, J. A.: Ice-sheet grounding-zone wedges (GZWs) on high-latitude continental margins, Marine Geol., 363, 65–92, https://doi.org/10.1016/j.margeo.2015.02.001, 2015.

Borchers, A., Dietze, E., Kuhn, G., Esper, O., Voigt, I., Hartmann, K., and Diekmann, B.: Holocene ice dynamics and bottom-water formation associated with Cape Darnley polynya activity recorded in Burton Basin, East Antarctica, Mar Geophys Res, 37, 49–70, https://doi.org/10.1007/s11001-015-9254-z, 2016.

Bradley, A. T. and Hewitt, I. J.: Tipping point in ice-sheet grounding-zone melting due to ocean water intrusion, Nat. Geosci., https://doi.org/10.1038/s41561-024-01465-7, 2024.

CALIB rev. 8; Stuiver, M., and Reimer, P.J., 1993, Radiocarb.,35, 215-230.

Domack, E., O'Brien, P., Harris, P., Taylor, F., Quilty, P. G., Santis, L. D., and Raker, B.: Late Quaternary sediment facies in Prydz Bay, East Antarctica and their relationship to glacial advance onto the continental shelf, Ant. Sci., 10, 236–246, https://doi.org/10.1017/S0954102098000339, 1998.

https://doi.org/10.5194/egusphere-2025-2515
Preprint. Discussion started: 10 July 2025

Dorschel, B., Hehemann, L., Viquerat, S., Warnke, F., Dreutter, S., Schulze Tenberge, Y., Accettella, D., An, L., Barrios, F., Bazhenova, E. A., Black, J., Bohoyo, F., Davey, C., de Santis, L., Escutia Dotti, C., Frémand, A. C., Fretwell, P. T., Gales, J. A., Gao, J., Gasperini, L., Greenbaum, J. S., Henderson Jencks, J., Hogan, K. A., Hong, J. K., Jakobsson, M., Jensen, L., Kool, J., Larin, S., Larter, R. D., Leitchenkov, G. L., Loubrieu, B., Mackay, K., Mayer, L., Millan, R., Morlighem, M., Navidad, F., Nitsche, F.-O., Nogi, Y., Pertuisot, C., Post, A. L., Pritchard, H. D., Purser, A., Rebesco, M., Rignot, E., Roberts, J. L., Rovere, M., Ryzhov, I., Sauli, C., Schmitt, T., Silvano, A., Smith, J. E., Snaith, H., Tate, A. J., Tinto, K., Vandenbossche, P., Weatherall, P., Wintersteller, P., Yang, C., Zhang, T., and Arndt, J. E.: The International Bathymetric Chart of the Southern Ocean Version 2 (IBCSO v2), PANGAEA [data set], https://doi.org/10.1594/PANGAEA.937574, 2022.

Dowdeswell, J. A. and Fugelli, E. M. G.: The seismic architecture and geometry of grounding-zone wedges formed at the marine margins of past ice sheets, Geol Soc Am Bull, 124, 1750–1761, https://doi.org/10.1130/B30628.1, 2012.

Dowdeswell, J. A., Canals, M., Jakobsson, M., Todd, B. J., Dowdeswell, E. K., and Hogan, K. A.: The variety and distribution of submarine glacial landforms and implications for ice-sheet reconstruction, J. Geol. Soc, Memoirs, 46, 519–552, https://doi.org/10.1144/M46.183, 2016.

Dowdeswell, J.A. & Hogan, K.A. 2016. Huge iceberg ploughmarks and associated corrugation ridges on the northern Svalbard shelf. In: Atlas of Submarine Glacial Landforms: Modern, Quaternary and Ancient., J. Geol. Soc , Memoirs, 46, 269 – 270, http://doi.org/10.1144/M46.4

Eaves, S. R., Mackintosh, A. N., Pedro, J. B., Bostock, H. C., Ryan, M. T., Norton, K. P., Hayward, B. W., Anderson, B. M., He, F., Jones, R. S., Lorrey, A. M., Newnham, R. M., Tims, S. G., and Vandergoes, M. J.: Coupled atmosphere-ocean response of the southwest Pacific to deglacial changes in Atlantic meridional overturning circulation, Earth Planet. Sci. Lett., 641, 118802, https://doi.org/10.1016/j.epsl.2024.118802, 2024.

Fretwell, P., Pritchard, H. D., Vaughan, D. G., Bamber, J. L., Barrand, N. E., Bell, R., Bianchi, C., Bingham, R. G., Blankenship, D. D., Casassa, G., Catania, G., Callens, D., Conway, H., Cook, A. J., Corr, H. F. J., Damaske, D., Damm, V., Ferraccioli, F., Forsberg, R., Fujita, S., Gim, Y., Gogineni, P., Griggs, J. A., Hindmarsh, R. C. A., Holmlund, P., Holt, J. W., Jacobel, R. W., Jenkins, A., Jokat, W., Jordan, T., King, E. C., Kohler, J., Krabill, W., Riger-Kusk, M., Langley, K. A., Leitchenkov, G., Leuschen, C., Luyendyk, B. P., Matsuoka, K., Mouginot, J., Nitsche, F. O., Nogi, Y., Nost, O. A., Popov, S. V., Rignot, E., Rippin, D. M., Rivera, A., Roberts, J., Ross, N., Siegert, M. J., Smith, A. M., Steinhage, D., Studinger, M., Sun, B., Tinto, B. K., Welch, B. C., Wilson, D., Young, D. A., Xiangbin, C., and Zirizzotti, A.: Bedmap2: improved ice bed, surface and thickness datasets for Antarctica, Cryosphere, 7, 375–393, https://doi.org/10.5194/tc-7-375-2013, 2013.

Golledge, N. R., Menviel, L., Carter, L., Fogwill, C. J., England, M. H., Cortese, G., and Levy, R. H.: Antarctic contribution to meltwater pulse 1A from reduced Southern Ocean overturning, Nat Commun, 5, 5107, https://doi.org/10.1038/ncomms6107, 2014.

Graham, A. G. C., Larter, R. D., Gohl, K., Hillenbrand, C.-D., Smith, J. A., and Kuhn, G.: Bedform signature of a West Antarctic palaeo-ice stream reveals a multi-temporal record of flow and substrate control, QSR, 28, 2774–2793, https://doi.org/10.1016/j.quascirev.2009.07.003, 2009.

https://doi.org/10.5194/egusphere-2025-2515
Preprint. Discussion started: 10 July 2025

Guitard, M. E., Shevenell, A. E., Lavoie, C., and Domack, E. W.: Mega-scale glacial lineations and grounding-zone wedges in Prydz Channel, East Antarctica, J. Geol. Soc , Memoirs, 46, 185–186, https://doi.org/10.1144/M46.110, 2016.

Harris, P. T. and O'Brien, P. E.: Bottom currents, sedimentation and ice-sheet retreat facies successions on the Mac Robertson shelf, East Antarctica, Mar. Geol. 151, 47–72, https://doi.org/10.1016/S0025-3227(98)00047-4, 1998.

Hauck, J., Gerdes, D., Hillenbrand, C.-D., Hoppema, M., Kuhn, G., Nehrke, G., Völker, C., and Wolf-Gladrow, D. A.: Distribution and mineralogy of carbonate sediments on Antarctic shelves, J. Mar. Syst, 90, 77–87, https://doi.org/10.1016/j.jmarsys.2011.09.005, 2012.

Heaton, T. J., Butzin, M., Bard, E., Bronk Ramsey, C., Hughen, K. A., Köhler, P., & Reimer, P. J.: MARINE RADIOCARBON CALIBRATION IN POLAR REGIONS: A SIMPLE APPROXIMATE APPROACH USING MARINE20. Radiocarbon, 65(4), 848–875. doi:10.1017/RDC.2023.42. 2023.

Hemer, M. A. and Harris, P. T.: Sediment core from beneath the Amery Ice Shelf, East Antarctica, suggests mid-Holocene ice-shelf retreat, Geol, 31, 127, https://doi.org/10.1130/0091-7613(2003)031<0127:SCFBTA>2.0.CO;2, 2003.

Hillenbrand, C.-D., Larter, R. D., Dowdeswell, J. A., Ehrmann, W., Ó Cofaigh, C., Benetti, S., Graham, A. G. C., and Grobe, H.: The sedimentary legacy of a palaeo-ice stream on the shelf of the southern Bellingshausen Sea: Clues to West Antarctic glacial history during the Late Quaternary, QSR, 29, 2741–2763, https://doi.org/10.1016/j.quascirev.2010.06.028, 2010.

Hillenbrand, C.-D., Bentley, M. J., Stolldorf, T. D., Hein, A. S., Kuhn, G., Graham, A. G. C., Fogwill, C. J., Kristoffersen, Y., Smith, James. A., Anderson, J. B., Larter, R. D., Melles, M., Hodgson, D. A., Mulvaney, R., and Sugden, D. E.: Reconstruction of changes in the Weddell Sea sector of the Antarctic Ice Sheet since the Last Glacial Maximum, QSR, 100, 111–136, https://doi.org/10.1016/j.quascirev.2013.07.020, 2014.

Hodgson, D. A., Graham, A. G. C., Roberts, S. J., Bentley, M. J., Cofaigh, C. Ó., Verleyen, E., Vyverman, W., Jomelli, V., Favier, V., Brunstein, D., Verfaillie, D., Colhoun, E. A., Saunders, K. M., Selkirk, P. M., Mackintosh, A., Hedding, D. W., Nel, W., Hall, K., McGlone, M. S., Van Der Putten, N., Dickens, W. A., and Smith, J. A.: Terrestrial and submarine evidence for the extent and timing of the Last Glacial Maximum and the onset of deglaciation on the maritime-Antarctic and sub-Antarctic islands, QSR, 100, 137–158, https://doi.org/10.1016/j.quascirev.2013.12.001, 2014.

Jakobsson, M., Anderson, J. B., Nitsche, F. O., Gyllencreutz, R., Kirshner, A. E., Kirchner, N., O'Regan, M., Mohammad, R., and Eriksson, B.: Ice sheet retreat dynamics inferred from glacial morphology of the central Pine Island Bay Trough, West Antarctica, QSR, 38, 1–10, https://doi.org/10.1016/j.quascirev.2011.12.017, 2012.

Jakobsson, M., Anderson, J. B., Nitsche, F. O., Dowdeswell, J. A., Gyllencreutz, R., Kirchner, N., Mohammad, R., O'Regan, M., Alley, R. B., Anandakrishnan, S., Eriksson, B., Kirshner, A., Fernandez, R., Stolldorf, T., Totten, R., and Majewski, W.: Geological record of ice shelf break-up and grounding line retreat, Pine Island Bay, West Antarctica, Geol., 39, 691–694, https://doi.org/10.1130/G32153.1, 2011.

Kawamata, M., Suganuma, Y., Doi, K., Misawa, K., Hirabayashi, M., Hattori, A., and Sawagaki, T.: Abrupt Holocene ice-sheet thinning along the southern Soya Coast, Lützow-Holm Bay, East Antarctica, revealed by glacial geomorphology and surface exposure dating, QSR, 247, 106540, https://doi.org/10.1016/j.quascirev.2020.106540, 2020.

https://doi.org/10.5194/egusphere-2025-2515
Preprint. Discussion started: 10 July 2025

King, E. C., Hindmarsh, R. C. A., and Stokes, C. R.: Formation of mega-scale glacial lineations observed beneath a West Antarctic ice stream, Nat. Geosci, 2, 585–588, https://doi.org/10.1038/ngeo581, 2009.

Klages, J. P., Kuhn, G., Hillenbrand, C.-D., Graham, A. G. C., Smith, J. A., Larter, R. D., Gohl, K., and Wacker, L.: Retreat of the West Antarctic Ice Sheet from the western Amundsen Sea shelf at a pre- or early LGM stage, QSR, 91, 1–15, https://doi.org/10.1016/j.quascirev.2014.02.017, 2014.

Klages, J. P., Kuhn, G., Graham, A. G. C., Hillenbrand, C.-D., Smith, J. A., Nitsche, F. O., Larter, R. D., and Gohl, K.: Palaeo-ice stream pathways and retreat style in the easternmost Amundsen Sea Embayment, West Antarctica, revealed by combined multibeam bathymetric and seismic data, Geomorphology, 245, 207–222, https://doi.org/10.1016/j.geomorph.2015.05.020, 2015.

Klages, J. P., Kuhn, G., Hillenbrand, C.-D., Smith, J. A., Graham, A. G. C., Nitsche, F. O., Frederichs, T., Jernas, P. E., Gohl, K., and Wacker, L.: Limited grounding-line advance onto the West Antarctic continental shelf in the easternmost Amundsen Sea Embayment during the last glacial period, PLoS ONE, 12, e0181593, https://doi.org/10.1371/journal.pone.0181593, 2017.

Larter, R. D., Anderson, J. B., Graham, A. G. C., Gohl, K., Hillenbrand, C.-D., Jakobsson, M., Johnson, J. S., Kuhn, G., Nitsche, F. O., Smith, J. A., Witus, A. E., Bentley, M. J., Dowdeswell, J. A., Ehrmann, W., Klages, J. P., Lindow, J., Cofaigh, C. Ó., and Spiegel, C.: Reconstruction of changes in the Amundsen Sea and Bellingshausen Sea sector of the West Antarctic Ice Sheet since the Last Glacial Maximum, QSR, 100, 55–86, https://doi.org/10.1016/j.quascirev.2013.10.016, 2014.

Leventer, A., Domack, E., Dunbar, R., Pike, J., Stickley, C., Maddison, E., Brachfeld, S., Manley, P., and McClennen, C.: Marine sediment record from the East Antarctic margin reveals dynamics of ice sheet recession, Gsa Today, 16, 4, https://doi.org/10.1130/GSAT01612A.1, 2006.

Lowe, A. and Anderson, J.: Reconstruction of the West Antarctic ice sheet in Pine Island Bay during the Last Glacial Maximum and its subsequent retreat history, QSR, 21, 1879–1897, https://doi.org/10.1016/S0277-3791(02)00006-9, 2002.

Mackintosh, A., White, D., Fink, D., Gore, D. B., Pickard, J., and Fanning, P. C.: Exposure ages from mountain dipsticks in Mac. Robertson Land, East Antarctica, indicate little change in ice-sheet thickness since the Last Glacial Maximum, Geol, 35, 551, https://doi.org/10.1130/G23503A.1, 2007.

Mackintosh, A., Golledge, N., Domack, E., Dunbar, R., Leventer, A., White, D., Pollard, D., DeConto, R., Fink, D., Zwartz, D., Gore, D., and Lavoie, C.: Retreat of the East Antarctic ice sheet during the last glacial termination, Nat. Geosci, 4, 195–202, https://doi.org/10.1038/ngeo1061, 2011.

Mackintosh, A. N., Verleyen, E., O'Brien, P. E., White, D. A., Jones, R. S., McKay, R., Dunbar, R., Gore, D. B., Fink, D., Post, A. L., Miura, H., Leventer, A., Goodwin, I., Hodgson, D. A., Lilly, K., Crosta, X., Golledge, N. R., Wagner, B., Berg, S., Van Ommen, T., Zwartz, D., Roberts, S. J., Vyverman, W., and Masse, G.: Retreat history of the East Antarctic Ice Sheet since the Last Glacial Maximum, QSR, 100, 10–30, https://doi.org/10.1016/j.quascirev.2013.07.024, 2014.

Majewski, W., Prothro, L. O., Simkins, L. M., Demianiuk, E. J., and Anderson, J. B.: Foraminiferal Patterns in Deglacial Sediment in the Western Ross Sea, Antarctica: Life Near Grounding Lines, Paleoceanog and Paleoclimatol, 35, e2019PA003716, https://doi.org/10.1029/2019PA003716, 2020.

https://doi.org/10.5194/egusphere-2025-2515
Preprint. Discussion started: 10 July 2025

Matsuoka, K., Skoglund, A., Roth, G., De Pomereu, J., Griffiths, H., Headland, R., Herried, B., Katsumata, K., Le Brocq, A., Licht, K., Morgan, F., Neff, P. D., Ritz, C., Scheinert, M., Tamura, T., Van De Putte, A., Van Den Broeke, M., Von Deschwanden, A., Deschamps-Berger, C., Van Liefferinge, B., Tronstad, S., and Melvær, Y.: Quantarctica, an integrated mapping environment for Antarctica, the Southern Ocean, and sub-Antarctic islands, Environ. Model.Softw, 140, 105015, https://doi.org/10.1016/j.envsoft.2021.105015, 2021.

Mizuta, G., Ohshima, K. I., Takatsuka, T., Kitade, Y., Fujii, M., Nakayama, Y., and Ikehara, M.: Circulation and production of Cape Darnley Bottom Water on the continental slope off the Cape Darnley polynya, East Antarctica, Deep Sea Research Part I: ORP, 211, 104362, https://doi.org/10.1016/j.dsr.2024.104362, 2024.

Mollenhauer, G., Grotheer, H., Gentz, T., Bonk, E., and Hefter, J.: Standard operation procedures and performance of the MICADAS radiocarbon laboratory at Alfred Wegener Institute (AWI), Germany, Nuclear Instruments and Methods in Physics Research Section B: Beam Interactions with Materials and Atoms, 496, 45–51, https://doi.org/10.1016/j.nimb.2021.03.016, 2021.

Morlighem, M., Rignot, E., Binder, T., Blankenship, D., Drews, R., Eagles, G., Eisen, O., Ferraccioli, F., Forsberg, R., Fretwell, P., Goel, V., Greenbaum, J. S., Gudmundsson, H., Guo, J., Helm, V., Hofstede, C., Howat, I., Humbert, A., Jokat, W., Karlsson, N. B., Lee, W. S., Matsuoka, K., Millan, R., Mouginot, J., Paden, J., Pattyn, F., Roberts, J., Rosier, S., Ruppel, A., Seroussi, H., Smith, E. C., Steinhage, D., Sun, B., Broeke, M. R. V. D., Ommen, T. D. V., Wessem, M. V., and Young, D. A.: Deep glacial troughs and stabilizing ridges unveiled beneath the margins of the Antarctic ice sheet, Nat. Geosci., 13, 132–137, https://doi.org/10.1038/s41561-019-0510-8, 2020.

Ó Cofaigh, C., Davies, B. J., Livingstone, S. J., Smith, J. A., Johnson, J. S., Hocking, E. P., Hodgson, D. A., Anderson, J. B., Bentley, M. J., Canals, M., Domack, E., Dowdeswell, J. A., Evans, J., Glasser, N. F., Hillenbrand, C.-D., Larter, R. D., Roberts, S. J., and Simms, A. R.: Reconstruction of ice-sheet changes in the Antarctic Peninsula since the Last Glacial Maximum, QSR, 100, 87–110, https://doi.org/10.1016/j.quascirev.2014.06.023, 2014.

Ohshima, K. I., Fukamachi, Y., Williams, G. D., Nihashi, S., Roquet, F., Kitade, Y., Tamura, T., Hirano, D., Herraiz-Borreguero, L., Field, I., Hindell, M., Aoki, S., and Wakatsuchi, M.: Antarctic Bottom Water production by intense sea-ice formation in the Cape Darnley polynya, Nat. Geosci, 6, 235–240, https://doi.org/10.1038/ngeo1738, 2013.

Pedro, J. B., Bostock, H. C., Bitz, C. M., He, F., Vandergoes, M. J., Steig, E. J., Chase, B. M., Krause, C. E., Rasmussen, S. O., Markle, B. R., and Cortese, G.: The spatial extent and dynamics of the Antarctic Cold Reversal, Nat. Geosci, 9, 51–55, https://doi.org/10.1038/ngeo2580, 2016.

Pritchard, H. D., Fretwell, P. T., Fremand, A. C., Bodart, J. A., Kirkham, J. D., Aitken, A., Bamber, J., Bell, R., Bianchi, C., Bingham, R. G., Blankenship, D. D., Casassa, G., Christianson, K., Conway, H., Corr, H. F. J., Cui, X., Damaske, D., Damm, V., Dorschel, B., Drews, R., Eagles, G., Eisen, O., Eisermann, H., Ferraccioli, F., Field, E., Forsberg, R., Franke, S., Goel, V., Gogineni, S. P., Greenbaum, J., Hills, B., Hindmarsh, R. C. A., Hoffman, A. O., Holschuh, N., Holt, J. W., Humbert, A., Jacobel, R. W., Jansen, D., Jenkins, A., Jokat, W., Jong, L., Jordan, T. A., King, E. C., Kohler, J., Krabill, W., Maton, J., Gillespie, M. K., Langley, K., Lee, J., Leitchenkov, G., Leuschen, C., Luyendyk, B., MacGregor, J. A., MacKie, E., Moholdt,

https://doi.org/10.5194/egusphere-2025-2515
Preprint. Discussion started: 10 July 2025

G., Matsuoka, K., Morlighem, M., Mouginot, J., Nitsche, F. O., Nost, O. A., Paden, J., Pattyn, F., Popov, S., Rignot, E., Rippin, D. M., Rivera, A., Roberts, J. L., Ross, N., Ruppel, A., Schroeder, D. M., Siegert, M. J., Smith, A. M., Steinhage, D., Studinger, M., Sun, B., Tabacco, I., Tinto, K. J., Urbini, S., Vaughan, D. G., Wilson, D. S., Young, D. A., and Zirizzotti, A.: Bedmap3 updated ice bed, surface and thickness gridded datasets for Antarctica, Sci Data, 12, 414, https://doi.org/10.1038/s41597-025-04672-y, 2025.

Reinardy, B. T. I., Hiemstra, J. F., Murray, T., Hillenbrand, C.-D., and Larter, R. D.: Till genesis at the bed of an Antarctic Peninsula palaeo-ice stream as indicated by micromorphological analysis: Till genesis at the bed of an Antarctic Peninsula palaeo-ice stream, Boreas, 40, 498–517, https://doi.org/10.1111/j.1502-3885.2010.00199.x, 2011.

Rignot, E., Mouginot, J., and Scheuchl, B.: Ice Flow of the Antarctic Ice Sheet, Sci., 333, 1427–1430, https://doi.org/10.1126/science.1208336, 2011.

Rignot, E., Mouginot, J., Scheuchl, B., Van Den Broeke, M., Van Wessem, M. J., and Morlighem, M.: Four decades of Antarctic Ice Sheet mass balance from 1979–2017, Proc. Natl. Acad. Sci. U.S.A., 116, 1095–1103, https://doi.org/10.1073/pnas.1812883116, 2019.

Sedwick, P. N., Harris, P. T., Robertson, L. G., McMurtry, G. M., Cremer, M. D., and Robinson, P.: Holocene sediment records from the continental shelf of Mac. Robertson Land, East Antarctica, Paleoceanography, 16, 212–225, https://doi.org/10.1029/2000PA000504, 2001.

Schoof, C.: Ice sheet grounding line dynamics: Steady states, stability, and hysteresis, J. Geophys. Res., 112, 2006JF000664, https://doi.org/10.1029/2006JF000664, 2007.

Smith, J. A., Graham, A. G. C., Post, A. L., Hillenbrand, C.-D., Bart, P. J., and Powell, R. D.: The marine geological imprint of Antarctic ice shelves, Nat Commun, 10, 5635, https://doi.org/10.1038/s41467-019-13496-5, 2019.

Schmidt, C., Morrison, A. K., and England, M. H.: Wind– and Sea-Ice–Driven Interannual Variability of Antarctic Bottom Water Formation, JGR Oceans, 128, e2023JC019774, https://doi.org/10.1029/2023JC019774, 2023.

The IMBIE team: Mass balance of the Antarctic Ice Sheet from 1992 to 2017, Nat., 558, 219–222, https://doi.org/10.1038/s41586-018-0179-y, 2018.

The RAISED Consortium. Bentley, M. J., Ó Cofaigh, C., Anderson, J. B., Conway, H., Davies, B., Graham, A. G. C., Hillenbrand, C.-D., Hodgson, D. A., Jamieson, S. S. R., Larter, R. D., Mackintosh, A., Smith, J. A., Verleyen, E., Ackert, R. P., Bart, P. J., Berg, S., Brunstein, D., Canals, M., Colhoun, E. A., Crosta, X., Dickens, W. A., Domack, E., Dowdeswell, J. A., Dunbar, R., Ehrmann, W., Evans, J., Favier, V., Fink, D., Fogwill, C. J., Glasser, N. F., Gohl, K., Golledge, N. R., Goodwin, I., Gore, D. B., Greenwood, S. L., Hall, B. L., Hall, K., Hedding, D. W., Hein, A. S., Hocking, E. P., Jakobsson, M., Johnson, J. S., Jomelli, V., Jones, R. S., Klages, J. P., Kristoffersen, Y., Kuhn, G., Leventer, A., Licht, K., Lilly, K., Lindow, J., Livingstone, S. J., Massé, G., McGlone, M. S., McKay, R. M., Melles, M., Miura, H., Mulvaney, R., Nel, W., Nitsche, F. O., O'Brien, P. E., Post, A. L., Roberts, S. J., Saunders, K. M., Selkirk, P. M., Simms, A. R., Spiegel, C., Stolldorf, T. D., Sugden, D. E., Van Der Putten, N., Van Ommen, T., Verfaillie, D., Vyverman, W., Wagner, B., White, D. A., Witus, A. E., and Zwartz,

https://doi.org/10.5194/egusphere-2025-2515
Preprint. Discussion started: 10 July 2025

D.: A community-based geological reconstruction of Antarctic Ice Sheet deglaciation since the Last Glacial Maximum, QSR, 100, 1–9, https://doi.org/10.1016/j.quascirev.2014.06.025, 2014.

Thompson, A. F., Stewart, A. L., Spence, P., and Heywood, K. J.: The Antarctic Slope Current in a Changing Climate, Rev. Geophys, 56, 741–770, https://doi.org/10.1029/2018RG000624, 2018.

Tiedemann, R. and Müller, J.: The Expedition PS128 of the Research Vessel POLARSTERN to the Lazarew Sea, Riiser-Larsen Sea, Cosmonaut Sea, and Cooperation Sea in 2022, n.d.

Wellner, J. S., Heroy, D. C., and Anderson, J. B.: The death mask of the antarctic ice sheet: Comparison of glacial geomorphic features across the continental shelf, Geomorphology, 75, 157–171, https://doi.org/10.1016/j.geomorph.2005.05.015, 2006.

Wong, A. P. S. and Riser, S. C.: Modified shelf water on the continental slope north of Mac Robertson Land, East Antarctica, Geophys. Res. Lett.., 40, 6186–6190, https://doi.org/10.1002/2013GL058125, 2013.